DOI: 10.1534/genetics.105.046359

Interactions of UNC-34 Enabled With Rac GTPases and the NIK Kinase MIG-15 in *Caenorhabditis elegans* Axon Pathfinding and Neuronal Migration

M. Afaq Shakir, Jason S. Gill and Erik A. Lundquist[1]

Department of Molecular Biosciences, University of Kansas, Lawrence, Kansas 66045

Manuscript received June 2, 2005
Accepted for publication September 21, 2005

ABSTRACT

Many genes that affect axon pathfinding and cell migration have been identified. Mechanisms by which these genes and the molecules they encode interact with one another in pathways and networks to control developmental events are unclear. Rac GTPases, the cytoskeletal signaling molecule Enabled, and NIK kinase have all been implicated in regulating axon pathfinding and cell migration. Here we present evidence that, in *Caenorhabditis elegans*, three Rac GTPases, CED-10, RAC-2, and MIG-2, define three redundant pathways that each control axon pathfinding, and that the NIK kinase MIG-15 acts in each Rac pathway. Furthermore, we show that the Enabled molecule UNC-34 defines a fourth partially redundant pathway that acts in parallel to Rac/MIG-15 signaling in axon pathfinding. Enabled and the three Racs also act redundantly to mediate AQR and PQR neuronal cell migration. The Racs and UNC-34 Ena might all control the formation of actin-based protrusive structures (lamellipodia and filopodia) that mediate growth cone outgrowth and cell migration. MIG-15 does not act with the three Racs in execution of cell migration. Rather, MIG-15 affects direction of PQR neuronal migration, similar to UNC-40 and DPY-19, which control initial Q cell polarity, and Wnt signaling, which acts later to control Q cell-directed migration. MIG-2 Rac, which acts with CED-10 Rac, RAC-2 Rac, and UNC-34 Ena in axon pathfinding and cell migration, also acts with MIG-15 in PQR directional migration.

IN the developing nervous system, nascent neurons must form axons, thin extensions of plasma membrane that make precise connections with targets in the nervous system. Axons are guided to their targets by the growth cone, a dynamic motile structure that detects and responds to extracellular guidance cues. These cues are detected by transmembrane receptor proteins on the surface of the growth cone and translated into changes in the dynamics and organization of the growth cone actin cytoskeleton, which underlies growth cone motility and guidance (Tessier-Lavigne and Goodman 1996; Dickson 2002; Gallo and Letourneau 2004). In addition to axon extension, neurons must often migrate from their birthplaces to their final positions in the organism. For example, neurons born in the germinal layers of the mammalian cerebrum migrate to distal layers in the cerebral cortex (Hatten 2002; Kriegstein and Noctor 2004). The process of cell migration is similar to growth cone outgrowth both morphologically and molecularly: both growth cones and leading edges of migrating cells consist of dynamic, actin-based plasma membrane protrusions called lamellipodia and filopodia; and many of the molecules that control growth cone outgrowth also control cell migration (*e.g.*, guidance receptors and cytoskeletal signaling molecules). Many guidance receptors and their ligands have been identified (Huber *et al.* 2003), and recent studies have uncovered many of the cytoplasmic signaling molecules that link guidance receptors to the actin cytoskeleton. The challenge remains to understand how pathfinding molecules work together in pathways and networks to mediate growth cone motility and cell migration. Here we demonstrate interactions between three previously identified signaling molecules that affect axon pathfinding: Rac small GTPases, the NIK kinase MIG-15, and the cytoskeletal signaling molecule UNC-34 Enabled.

Rac GTPases of the Rho subfamily regulate cell morphology and actin organization in many systems (Hall 1998). Genetic studies in Drosophila and *Caenorhabditis elegans* have pinpointed Rac GTPases as key regulators of growth cone outgrowth during axon pathfinding and cell migration (Luo 2000; Dickson 2001; Lundquist 2003). In *C. elegans*, three Rac-like GTPases CED-10 (Reddien and Horvitz 2000), RAC-2, and MIG-2 (Zipkin *et al.* 1997) act redundantly in axon pathfinding (no single Rac mutation strongly affects axon pathfinding, whereas pairwise double mutants have severe defects in axon pathfinding) (Lundquist *et al.* 2001). Here we show that two *ced-10* null alleles have little effect on axon pathfinding and neuronal migration on their own, confirming the idea that Rac GTPases have overlapping roles in axon pathfinding.

The *mig-15* encodes the *C. elegans* version of the vertebrate Nck-interacting kinase (NIK) and the Drosophila

[1]*Corresponding author:* Department of Molecular Biosciences, University of Kansas, 1200 Sunnyside Ave., 5049 Haworth Hall, Lawrence, KS 66045. E-mail: erikl@ku.edu

Misshapen protein (Poinat *et al.* 2002). MIG-15 contains an N-terminal STE20-like serine/threonine kinase domain and a regulatory C-terminal CNH domain, also found in the Citron protein in which it acts as a Rho GTPase effector domain (Madaule *et al.* 2000). Drosophila Misshapen and *C. elegans* MIG-15 have been shown to affect axon pathfinding and cell migration (Ruan *et al.* 1999; Su *et al.* 2000; Poinat *et al.* 2002). Indeed, a C-terminal region of *C. elegans* MIG-15 interacts with the cytoplasmic domain of the alpha integrin subunit INA-1, and genetic studies place the two molecules in the same pathway in VD/DD GABAergic motor neuron axon pathfinding (Poinat *et al.* 2002). RNA mediated interference (RNAi) of *ced-10* and *mig-2* enhance a weak *mig-15* mutation (Poinat *et al.* 2002), indicating that MIG-15 acts with the Racs in axon pathfinding of the VD/DD axons, although it is unclear if they act in the same or in parallel pathways.

The *unc-34* encodes the *C. elegans* Enabled (Ena) protein (Withee *et al.* 2004). Ena has been shown to control actin organization and cell shape in many systems (Krause *et al.* 2003), and *unc-34* null mutations affect axon pathfinding and neuronal migration in *C. elegans* (Gitai *et al.* 2003; Withee *et al.* 2004). Indeed, UNC-34 Ena is required for the ectopic neurite formation induced by an activated UNC-40 guidance receptor in the *C. elegans* AVM neuron and might act in parallel to CED-10 Rac in this process (Gitai *et al.* 2003).

Rac GTPases, MIG-15 NIK, and UNC-34 Ena all affect axon pathfinding and cell migration, but it is unclear how these molecules interact to control these processes. Here we present evidence confirming that *rac* null alleles have little effect on axon pathfinding and neuronal migration and that the three *rac* genes have overlapping roles in these processes. We present data indicating that MIG-15 NIK and the three Rac proteins act in the same pathway to control axon pathfinding and that UNC-34 Ena defines a parallel, partially overlapping pathway separate from the Rac pathway in the control of axon pathfinding. In addition to their roles in axon pathfinding, the Racs and UNC-34 Ena also have partially overlapping function in the migration of the AQR and PQR neurons, sensory neurons that undergo long-range migration in the larva. Rac and Enabled signaling might affect a common process in axon pathfinding and cell migration, possibly the formation of lamellipodia and filopodia that underlie growth cone outgrowth and cell migration.

While MIG-15 NIK acts with the Racs in axon pathfinding, data presented here indicate that MIG-15 NIK might not affect the ability of AQR and PQR neurons to execute migrations but instead might control direction of PQR neuronal migration. Neuronal cell polarity underlies multiple aspects of neuronal development including the location of axon initiation from the cell body as well as the direction of cell body migration. MIG-2 Rac but not CED-10 or RAC-2 Rac act with MIG-15 in control of PQR direction of migration.

MATERIALS AND METHODS

***C. elegans* genetics, transgenics, and genetic mapping:** *C. elegans* were cultured by standard techniques (Brenner 1974; Sulston and Hodgkin 1988). All experiments were performed at 20° unless otherwise noted. Germline transformation by gonadal micro-injection was performed by standard techniques (Mello and Fire 1995). RNAi of *rac-2* was performed as described previously (Lundquist *et al.* 2001). The following mutations and transgenic constructs were used in this work:

LGI: *dpy-5(e61), unc-40(e271)*
LGII: *juIs73[unc-25::gfp], dpy-10(e128)*
LGIII: *dpy-17(e124), mab-5(e1239), dpy-19(e1259)*
LGIV: *ced-10(n1993, n3246, n3417, lq20,* and *tm597), nT1 IV:V, dpy-13(e184), lqIs3[osm-6::gfp]*
LGV: *unc-34(e951, gm104, and lq17), dpy-11(e224)*
LGX: *szT1 X:I, lqIs2[osm-6::gfp], mig-2(mu28* and *lq13), unc-115(mn481* and *ky275), mig-15(rh148* and *rh80)*

The *lq17* mutation was assigned to a linkage group by analysis of segregation against a *dpy* mutation on each linkage group using the synthetic lethal phenotype of *lq17* with *ced-10(n1993). lq17* was found to segregate away from *dpy-11* on LGV, and showed independent assortment with *dpy-5 I, dpy-10 II, dpy-17 III, dpy-13 IV,* and the X chromosome (data not shown). Complementation tests with *unc-34(e951* and *gm104)* on LGV showed that *lq17* failed to complement *unc-34* and that *lq17* was an allele of *unc-34.*

Where possible, double mutants were maintained as homozygous stocks. In some cases, double mutant combinations were lethal or maternal-effect lethal and could not be maintained as homozygous lines. In these cases, one or both of the mutations was maintained in a heterozygous state over a closely linked mutation or a balancer chromosome: *ced-10* was balanced by the closely linked and semidominant *dpy-13(e184)* mutation or by the balancer *nT1 qIs51*; *unc-34* was also balanced by *nT1qIs51*; and *mig-15* was balanced by the balancer *szT1.* Double homozygotes from *nT1 qIs51* strains were detected by lack of green fluorescent protein (GFP) fluorescence in the pharynx (due to the *qIs51* integrated transgene on the *nT1* balancer), and *mig-15* homozygotes were selected from *szT1* strains by the uncoordinated and egg-laying-defective phenotype exhibited by *mig-15* alleles.

Scoring of PDE and VD/DD axon defects and AQR/PQR cell migration: Axon pathfinding defects and cell-positioning defects were scored in fourth larval stage (L4) or young pregravid adult animals harboring green fluorescent protein (*gfp*) transgenes expressed in specific cell types. PDE neurons and axons were visualized in animals harboring an *osm-6::gfp* transgene (*lqIs3 IV* or *lqIs2 X*) that is expressed in all ciliated sensory neurons including PDE, AQR, and PQR (Collet *et al.* 1998; Struckhoff and Lundquist 2003). A PDE axon was scored as misguided if it failed to directly extend to the ventral nerve cord (VNC). Those axons that grew at >45° angle to straight ventral were scored as misguided, whether the axon eventually reached the VNC or not. PDE neurons were scored as having ectopic neurites if processes in addition to the normal axon and dendrite were seen emanating from the PDE cell body or axon (axon branching).

VD/DD motor neuron morphology was scored in animals harboring an *unc-25::gfp* transgene (*juIs73 II*) (Jin *et al.* 1999), which is expressed in all GABAergic motor neurons including the VDs and DDs. Normally, VD/DD commissures extend directly from the VNC to the dorsal surface, where they form the dorsal nerve cord. In wild type, occasional minor misrouting of the VD/DD commissures is observed (not more than one or two per animal). The VD/DD commissural axon

pathfinding of an animal was scored as defective if more than two commissural axons were misguided, terminated prematurely, or extended extra axon branches. In most cases when VD/DD pathfinding was disrupted, the defects were very severe and affected most commissural processes.

AQR and PQR neuron positioning defects were scored in animals harboring an *osm-6::gfp* transgene. AQR is a descendant of the QR neuroblast, which is born in the right posterior-lateral region of the animal and initiates anterior migration (Sulston and Horvitz 1977). Along its route, QR divides to produce AQR as well as other descendant neurons AVM and SDQR. AQR continues anterior migration into the head of the animal near the posterior pharyngeal bulb. PQR is a descendant of the QL neuroblast, which is born in left posterior-lateral region of the animal and initiates a posterior migration. Along the way, QL divides to produce PQR and other descendant neurons PVM and SDQL. PQR continues posterior migration and finally resides among the left phasmid neurons in the tail of the animal. Defects in the direction of PQR migration were scored as misplacement of PQR to the anterior of the QL birthplace (PQR was considered anteriorly misplaced if it resided anterior to the vulva). The ability of AQR and PQR to execute migration was scored as defective if AQR or PQR failed to reach their final destinations, including complete failure of migration so that the AQR and PQR cell bodies resided at the Q cells' birthplaces (between the vulva and the PDE neurons).

For each of the phenotypic parameters described above, a percentage of defective axons or animals was derived. At least 100 animals of each genotype were scored for each phenotypic class, and a standard error of the proportion was calculated and represented by the error bars in the bar graphs.

Screen for *ced-10(n1993)* synthetic lethal mutations: To screen for new mutations that were synthetic lethal with *ced-10(n1993)*, we took advantage of the behavior of extrachromosomal arrays in *C. elegans*, which can be lost during meiosis such that some gametes do not inherit the array (*i.e.*, animals harboring an array give rise to both array-bearing progeny and progeny that have lost the array). We constructed an extrachromosomal array (called *lqEx246*) with the full-length *ced-10::gfp* transgene described previously (Lundquist *et al.* 2001). This transgene contains the *ced-10* promoter driving the expression of full-length CED-10 protein with GFP at the N terminus. This transgene rescued the cell corpse phagocytosis defects and distal tip cell migration defects of *ced-10(n1993)*, *ced-10(n3417)*, and *ced-10(tm597)* (data not shown), indicating that it produced a functional GFP::CED-10 molecule. Furthermore, *lqEx246* rescued the axon pathfinding defects of *ced-10(n1993); mig-2(mu28)* double mutants and the lethality of *ced-10(n3417* and *tm597)* and *mig-2(mu28); ced-10(n1993)* animals. *lqEx246* did not provide maternal *ced-10* activity, as *ced-10(n3417)*, *ced-10(tm597)*, and *ced-10(n1993); mig-2(mu28)* animals that did not inherit the array were zygotic embryonic lethal rather than maternal-effect lethal (*i.e.*, maternal-effect lethality was converted to embryonic lethality due to lack of maternal *gfp::ced-10* activity from *lqEx246*). Extrachromosomal arrays are often silenced in the germline and thus do not provide maternal gene activity (Kelly *et al.* 1997).

We used this transgene to screen for new EMS-induced mutations that were synthetic lethal with *ced-10*. Using standard techniques of ethyl methansulfonate (EMS) mutagenesis (Anderson 1995), we mutagenized *ced-10(n1993)* animals harboring the *gfp::ced-10* transgene in an extrachromosomal array (*ced-10(n1993); lqEx246* animals), allowed P0 hermaphrodites to self-fertilize, and placed individual F1 *ced-10(n1993); lqEx246* animals on single plates. Two F2 *ced-10; lqEx246* animals from each F1 were placed on single plates, and the F3 broods were inspected for GFP fluorescence. Normally, we observed both array-bearing (GFP+) and non-array-bearing (GFP-) adult F3 progeny from F2 animals. If, however, the F2 harbored a homozygous mutation that was synthetic lethal with *ced-10(n1993)*, we observed only array-bearing adult F3 and few non–array-bearing adults [*i.e.*, animals that lost *lqEx246* were now homozygous for both *ced-10(n1993)* and the new mutation and were lethal]. We screened the F2 progeny of 3500 F1 animals and found three mutations, *lq13*, *lq17*, and *lq20*, that displayed synthetic defects with *ced-10*. Through a combination of genetic mapping experiments using the synthetic lethality with *ced-10* and complementation tests with known genes, we determined that *lq13* was a new allele of *mig-2*, an expected result of the screen. We found that *lq20* was a new mutation in *ced-10* such that the *ced-10* gene in these animals carried both the *n1993* lesion and the *lq20* lesion. Finally, we determined that *lq17* was a novel allele of the *unc-34* gene, which encodes the *C. elegans* ortholog of Enabled.

Mapping of *mig-2(lq13)* and *ced-10(n1993lq20)*: We determined that *lq13* was linked to the X linkage group by crossing *lq13; ced-10(n1993)* hermaphrodites balanced with an extrachromosomal array bearing *ced-10(+)* DNA to *ced-10(n1993)* males and observing that all resulting adult male cross-progeny harbored the array and none had lost it (*i.e.*, males that lost the array were hemizygous for *lq13* and homozygous for *ced-10* and thus depended upon the *ced-10* activity provided by the array for their survival). Because *mig-2* is on the X linkage group and *mig-2* was previously known to be synthetic lethal with *ced-10(n1993)*, we conducted a complementation test with *mig-2(mu28)* and *lq13*. Upon outcrossing the *lq13; ced-10(n1993); array* strain to wild type, we noted that *lq13* homozygotes in a *ced-10(n1993)* heterozygous background [*lq13; ced-10(n1993)/+*] were strongly uncoordinated (Unc), indicating that loss of one copy of the *ced-10* gene enhanced *lq13* to cause uncoordination whereas loss of both copies of *ced-10* enhanced *lq13* to lethality. We crossed hemizygous *mig-2(mu28)* males to *lq13; ced-10(n1993); array* animals and found that all non–array-bearing cross-progeny hermaphrodites of the genotype *lq13/ mig-2(mu28); ced-10(n1993)/+* were strongly Unc, indicating that *mig-2(mu28)* failed to complement *lq13*.

Outcrossing and genetic mapping experiments indicated that the *lq20* mutation was tightly linked to *ced-10(n1993)* (*e.g.*, we could not recover the *n1993* allele alone from the *n1993lq20* strain). This prompted us to directly determine the nucleotide sequence of the *ced-10* gene in *n1993lq20* animals. *lq20* was a new allele in the *ced-10* gene itself (see results), and mutants carried both the *n1993* lesion and the *lq20* lesion in the *ced-10* gene.

Molecular biology: Recombinant DNA, polymerase chain reaction (PCR), and other molecular biology techniques were performed using standard procedures (Sambrook *et al.* 1989). All primer sequences used in PCR are available upon request. The molecular lesions associated with *mig-2(lq13)*, *ced-10 (n1993lq20)*, *unc-34(lq17)*, *mig-15(rh148)*, *mig-15(rh80)*, and *mig-15(rh326)* were identified as follows: the coding regions of each gene were amplified by PCR from genomic DNA isolated from the mutant strain. The PCR products were directly sequenced using gene-specific primers and standard techniques. The nucleotide sequence of each exon was determined, as well as the flanking intronic sequences (~30–50 nucleotides) to identify possible splice site mutations. The mutant sequence was compared to wild-type sequence and to the other mutant sequences to identify potential lesions. The sequencing procedure was repeated on each mutant to independently confirm the nature of the lesion. In each case, the lesion associated with a particular mutation was found in neither wild-type nor distinct mutant strains.

Construction and analysis of *mig-2* and *ced-10* mutant transgenes: The point mutations corresponding to *ced-10 (lq20* and *n3246)* and *mig-2(lq13)* were introduced into the

previously described *ced-10* and *mig-2* transgenes, respectively (Struckhoff and Lundquist 2003). The transgene consisted of the wild-type *ced-10* and *mig-2* coding region controlled by the *osm-6* promoter, which drives expression in ciliated sensory neurons including PDE. Point mutations were introduced into the coding regions of these transgenes by site-directed mutagenesis (Quikchange kit, Stratagene, La Jolla, CA). Animals were made transgenic with wild-type and mutant transgenes by gonadal micro-injection of a 1-ng/μl transgene solution with an *osm-6::gfp* transgene (25 ng/μl) as a transformation marker. Transformation with wild-type *ced-10* and *mig-2* transgenes at this concentration caused few PDE axon defects, whereas the mutant transgenes at this concentration caused significant PDE defects as well as slow growth and some lethality. In fact, these transgenes were difficult to maintain as stable lines and were gradually lost as they were transmitted, possibly due to selection against lethality and slow growth. Defects were noted in the first three generations after the initial transformation experiment.

Generation of *unc-34* cDNAs from *unc-34(lq17)* mutants: We used reverse transcription PCR (RT–PCR) to generate *unc-34* cDNAs from *unc-34(lq17)* mutants to assess the effect of *lq17* on *unc-34* splicing. We isolated total RNA from wild-type and *unc-34(lq17)* animals by standard techniques (Krause 1995) and subjected 1 μg of total RNA to reverse transcription using AMV reverse transcriptase and a primer specific to the *unc-34* 3′ UTR (see Figure 8B). Using a nested 3′ UTR primer and a 5′ primer specific to the start of the *unc-34* coding region (Figure 8B), we amplified *unc-34* RT products by PCR (35 cycles) and separated the PCR products by agarose gel electrophoresis. The ~1.4-kb RT–PCR products from wild type and *unc-34(lq17)* were sequenced directly using gene-specific primers and standard techniques. The RT–PCR was repeated twice to confirm these results.

Microscopy and imaging: Animals were mounted for microscopy in a drop of M9 buffer (Sulston and Hodgkin 1988) on a 2% agarose pad, both containing 5 mm sodium azide as an anesthetic. A coverslip was placed over the sample, and the slides were analyzed by epifluorescence microscopy for GFP or by differential interference contrast (DIC) microscopy (Leica DMR compound microscope). Images were captured by a Hamamatsu Orca digital camera and analyzed using Openlab software.

RESULTS

Null alleles of *ced-10 Rac* synergize with *mig-2 Rac* mutations and *rac-2(RNAi)* in axon pathfinding: Previous studies indicated that the null *mig-2(mu28)* allele and the hypomorphic *ced-10(n1993)* allele caused few axon defects on their own (Lundquist *et al.* 2001). However, *ced-10(n1993); mig-2(mu28)* double mutants displayed severe axon pathfinding defects, indicating that *ced-10* and *mig-2* have overlapping roles in axon pathfinding (Lundquist *et al.* 2001; Wu *et al.* 2002).

We characterized a new *ced-10* null allele. The *ced-10 (tm597)* allele (S. Mitani, National Bioresource Project for the Experimental Animal "Nematode *C. elegans*") was a 612-bp deletion of the *ced-10* locus that removed all of exon 2 and part of exon 3 (Figure 1A). The previously characterized *ced-10(n3417)* deletion removed all of exon 2 and 3 (Figure 1A) (Lundquist *et al.* 2001). Both *ced-10(n3417)* and *ced-10(tm597)* are likely to be *ced-10* null alleles. *ced-10(tm597)* animals displayed a phenotype similar to *ced-10(n3417)* animals: *tm597* animals were maternal-effect embryonic lethal with severe defects in morphogenesis, including early defects in gastrulation [a Gex phenotype (Soto *et al.* 2002)] and embryonic elongation (data not shown). *tm597* homozygotes with wild-type *ced-10* contribution were viable and had defects in gonad morphogenesis due to distal tip cell migration errors and defects in phagocytosis of cells undergoing programmed cell death (data not shown).

We analyzed the effects of *ced-10(tm597)* on pathfinding of the axons of two populations of neurons, the PDEs and the VD and DD motor neurons. The cell bodies of the bilateral PDE neurons reside in the posterior deirid ganglia in the posterior-lateral region of the animal and can be visualized and unambiguously identified with an *osm-6::gfp* transgene (Figure 2A) (Collet *et al.* 1998; Struckhoff and Lundquist 2003). The PDEs extend a single dendrite dorsally and a single unbranched axon straight ventrally to the VNC, where the axon bifurcates and extends anteriorly and posteriorly in the VNC (White *et al.* 1986). The VD and DD motor neuron cell bodies reside along the VNC and normally extend axons anteriorly in the VNC, which then turn dorsally and extend as single-axon commissures to the dorsal nerve cord (Figure 2C) (White *et al.* 1986). We found that *ced-10(tm597M+)* animals alone displayed few defects in PDE and VD/DD axon pathfinding (Figure 3A). Furthermore, *trans*-heterozygous combinations of *ced-10(tm597)*with *ced-10(n1993)* lacking maternal wild-type *ced-10*, which were viable and fertile, also showed few axon defects, similar to *ced-10(n3417)/ced-10(n1993)* (Figure 3A). Single mutant genotypes displayed some weak defects in VD/DD axon pathfinding [*e.g.*, *mig-2(mu28)* displayed 20%; Figure 3A]. However, these defects were not as severe as those seen in the double mutants described below. Thus, neither *ced-10(n3417)* nor *ced-10(tm597)*, both likely to be null mutations, had strong effects on PDE and VD/DD axon pathfinding.

We found that both *ced-10(n3417)* and *ced-10(tm597)* displayed severe axon defects in double mutant combinations with *mig-2(mu28)* (Figures 2 and 3A). Defects in PDE axon pathfinding in *ced-10(n3417M+); mig-2(mu28)* and *ced-10(tm597M+); mig-2(mu28)* double mutants included axon guidance errors, indicated by failure of the axon to extend directly to the VNC and instead wander laterally (69% and 72% of PDEs from *ced-10(n3417M+); mig-2(mu28)* and *ced-10(tm597M+); mig-2(mu28)*, respectively); and formation of ectopic neurites emanating from the cell body or from the axon (Figure 2B). Defects in VD/DD axon pathfinding in *ced-10(n3417M+); mig-2(mu28)* and *mig-2(mu28); ced-10(tm597M+)* double mutants included failed guidance, indicated by commissural axons that wandered laterally and sometimes failed to reach the dorsal cord; axon termination, when axon extension terminated

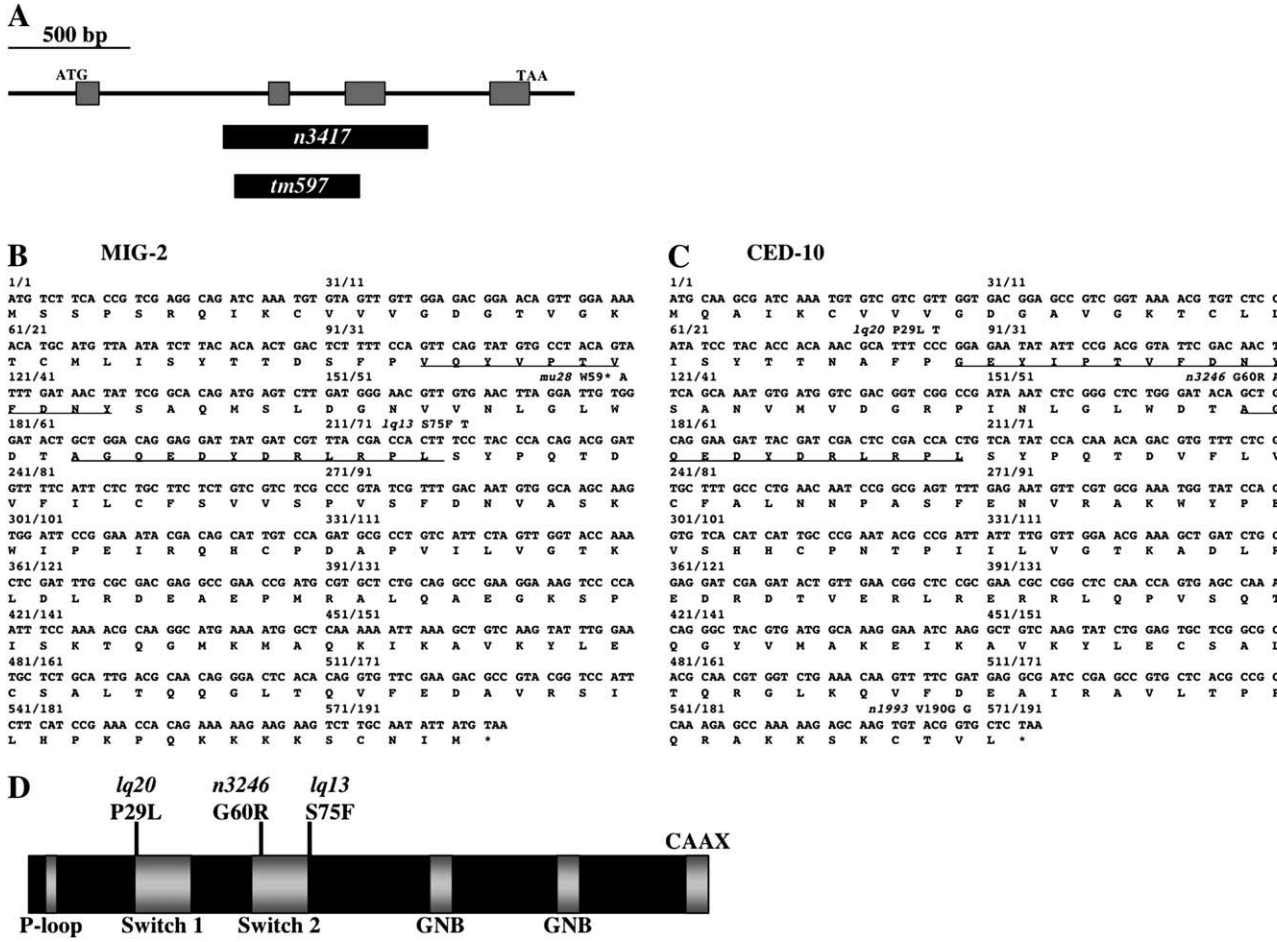

FIGURE 1.—Mutations in the *ced-10* and *mig-2* loci. (A) A diagram of the *ced-10* gene. Left to right is 5′–3′. Shaded boxes represent exons. The extents of two *ced-10* deletions are shown. *n3417* removes bases 34554 to 35530 and *tm597* removes bases 34880–35491 of the *ced-10* region relative to cosmid C09G12 (GenBank accession no. AF038608). (B and C) Nucleotide sequences of the *mig-2* and *ced-10* coding regions (GenBank accession nos. CAB01691 and AAC25821, respectively). The amino acid sequence is shown below the nucleotide sequence. Numbering represents nucleotide sequence/amino acid sequence. The switch 1 and switch 2 regions of the polypeptide sequence are underlined. Nucleotide lesions associated with each mutant are represented above the nucleotide sequence, as well as the allele name and the resulting amino acid substitution. *mig-2(mu28)* is a G179-to-A transition resulting in a premature stop codon; *mig-2(lq13)* is a C224-to-T transition resulting in an S75-to-F substitution; *ced-10(n1993)* is a T569-to-G transition resulting in a V190-to-G substitution; *ced-10(lq20)* is a C86-to-T transition resulting in a P29-to-L substitution; and *ced-10(n3246)* is a G178-to-A transition resulting in a G60-to-R substitution. (D) A diagram of general structure of MIG-2, CED-10, and RAC-2 GTPases. Indicated are the P-loop, the switch 1 and switch 2 regions, two guanine nucleotide binding domains (GNB) and the C-terminal CAAX sequence that mediates prenylation. MIG-2 has an N-terminal myristoylation sequence (not shown) that is not found on CED-10 or RAC-2. The relative locations of the *ced-10(lq20* and *n3246)* and *mig-2(lq13)* mutations are indicated.

prematurely before reaching the dorsal cord; and formation of ectopic neurites emanating from the commissural axon (Figures 2D and 3A). Every *ced-10(n3417M+); mig-2(mu28)* and *ced-10(tm597M+); mig-2(mu28)* mutant animal analyzed showed VD/DD axon pathfinding defects. A third Rac GTPase, RAC-2, acts redundantly with *ced-10(n1993)* and *mig-2(mu28)* (LUNDQUIST *et al.* 2001). We found that *ced-10(n3417)* and *ced-10(tm597)* animals treated with *rac-2* RNAi displayed similar but weaker axon pathfinding defects as described for the *mig-2* doubles (Figure 3A). We used RNAi to silence *rac-2* because neither of the two extant *rac-2* alleles caused a phenotype in double mutant combinations with *mig-2* and *ced-10* (E.A.L., unpublished results). We have strong evidence that *rac-2* RNAi specifically targets *rac-2* depletion (LUNDQUIST *et al.* 2001) and that the two *rac-2* alleles are not null (E.A.L., unpublished results). However, these results with *rac-2* RNAi should be interpreted with caution until the null phenotype of *rac-2* is clarified. With previous results, these data indicate that null alleles of neither *ced-10* nor *mig-2* strongly affect axon pathfinding and that *ced-10*, *mig-2*, and *rac-2* have overlapping roles in axon pathfinding.

***mig-2*, *ced-10*, and *rac-2* have overlapping roles in AQR and PQR neuronal migration:** Previous results

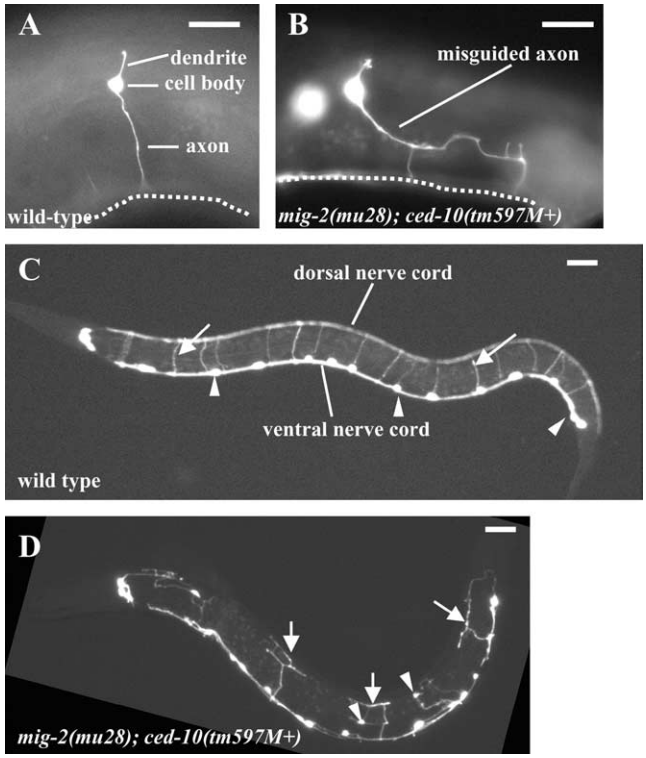

FIGURE 2.—Axon pathfinding defects of *ced-10(tm597); mig-2(mu28)* double mutants. (A and B) Fluorescent micrographs of fourth larval stage (L4) animals with *osm-6::gfp* expression in the PDE neuron. (C and D) Micrographs of L4 animals with *unc-25::gfp* expression in the VD and DD motor neurons. Anterior is left and dorsal is up. (A) A wild-type PDE neuron. The PDE axon extended directly to the ventral nerve cord (dashed line) without wandering or forming ectopic branches. (B) The PDE axon of a *mig-2(mu28); ced-10(tm597M+)* animal failed to extend directly to the ventral nerve cord, wandered laterally, and exhibited ectopic branches. (C) A wild-type animal. The VD and DD cell bodies resided along the ventral nerve cord (arrowheads) and the commissural axons extended directly to the dorsal nerve cord without wandering or exhibiting extra branches (arrows). (D) A *mig-2(mu28); ced-10(tm597M+)* animal. The commissural VD and DD axons wandered laterally, terminated prematurely without reaching the dorsal cord, and exhibited ectopic branches (arrows). VD or DD cell bodies were displaced laterally from their normal position in the ventral cord (arrowheads). Bars: A and B, 10 μm; C and D, 20 μm.

indicate that *ced-10*, *mig-2*, and *rac-2* have overlapping roles in migration of the CAN neurons (LUNDQUIST *et al.* 2001). We found that the three *rac* genes also redundantly control the migrations of the AQR and PQR neurons. The AQR neuron is born from the Q neuroblast on the right side of the animal (QR) in the posterior midbody region and migrates anteriorly to a position near the posterior pharynx (Figure 4A and MATERIALS AND METHODS). The PQR neuron is born from the left Q neuroblast (QL) and migrates posteriorly to a position near the phasmid neurons in the left lumbar ganglion (Figure 4A and MATERIALS AND METHODS). The Q cells respond to left-right asymmetry cues by extending processes anteriorly (QR) or posteriorly (QL), which polarizes the cells to migrate anteriorly or posteriorly, respectively (HONIGBERG and KENYON 2000). After an initial Q cell migration, Wnt signaling induces the expression of the *mab-5* gene in QL, which causes QL and its descendants to continue their posterior migrations (SALSER and KENYON 1992; MALOOF *et al.* 1999). QR and its descendants, which do not express *mab-5*, continue their anterior migrations. Mutations that disrupt the orientation of initial QL polarity and initial migration as well as those that disrupt later *mab-5* expression cause QL and/or its daughter cells to migrate anteriorly instead of posteriorly (HONIGBERG and KENYON 2000). We monitored PQR direction of migration by scoring misplacement of PQR anterior to the vulva, indicating that PQR or its precursors migrated anteriorly instead of posteriorly. We also monitored the ability of AQR and PQR to migrate along their normal routes by assaying misplacement of AQR and PQR along their correct migration routes (*e.g.*, a PQR neuron that migrated posteriorly but stopped before reaching its final destination near the phasmid neurons).

No single loss-of-function *rac* mutation strongly affected the direction of PQR migration or the ability of AQR and PQR to migrate (Figure 3B), although *mig-2(mu28)* showed weak but significant defective AQR and PQR migration along their normal routes (5%; Figure 3B), consistent with previous results demonstrating that *mig-2(mu28)* affects the migrations of other Q neuroblast daughters.

In pairwise double *rac* mutant combinations, including those with *rac-2(RNAi)* and the putative null *ced-10* deletion alleles, strong defects in AQR and PQR migration along their normal routes were observed (Figure 3B and Figure 4, B and C). For example, *ced-10(tm597M+)* and *mig-2(mu28)* alone showed 3% and 5% AQR/PQR migration defects respectively, whereas the *ced-10(tm597M+); mig-2(mu28)* double mutant displayed 67% AQR/PQR migration defects. The effects observed with *rac-2(RNAi)* were generally weaker than those observed with *ced-10* and *mig-2* mutations. Thus, *ced-10*, *mig-2*, and *rac-2* have overlapping roles in AQR and PQR neuronal migration. We detected no significant defect in the direction of PQR migration in these double mutants, suggesting that the three *rac* genes might have overlapping roles in the ability of AQR and PQR to migrate but not in the direction of PQR migration. We also observed lateral misplacement of VD/DD motor neuron cell bodies in double mutants (Figure 2D) consistent with previous results showing that the *rac* genes redundantly control the ventral migrations of the P cells, the progenitors of the VD and DD neurons (LUNDQUIST *et al.* 2001). The previously described constitutively active *mig-2(rh17)* allele (ZIPKIN *et al.* 1997) caused defects in PDE axon pathfinding and AQR and PQR migration (Figure

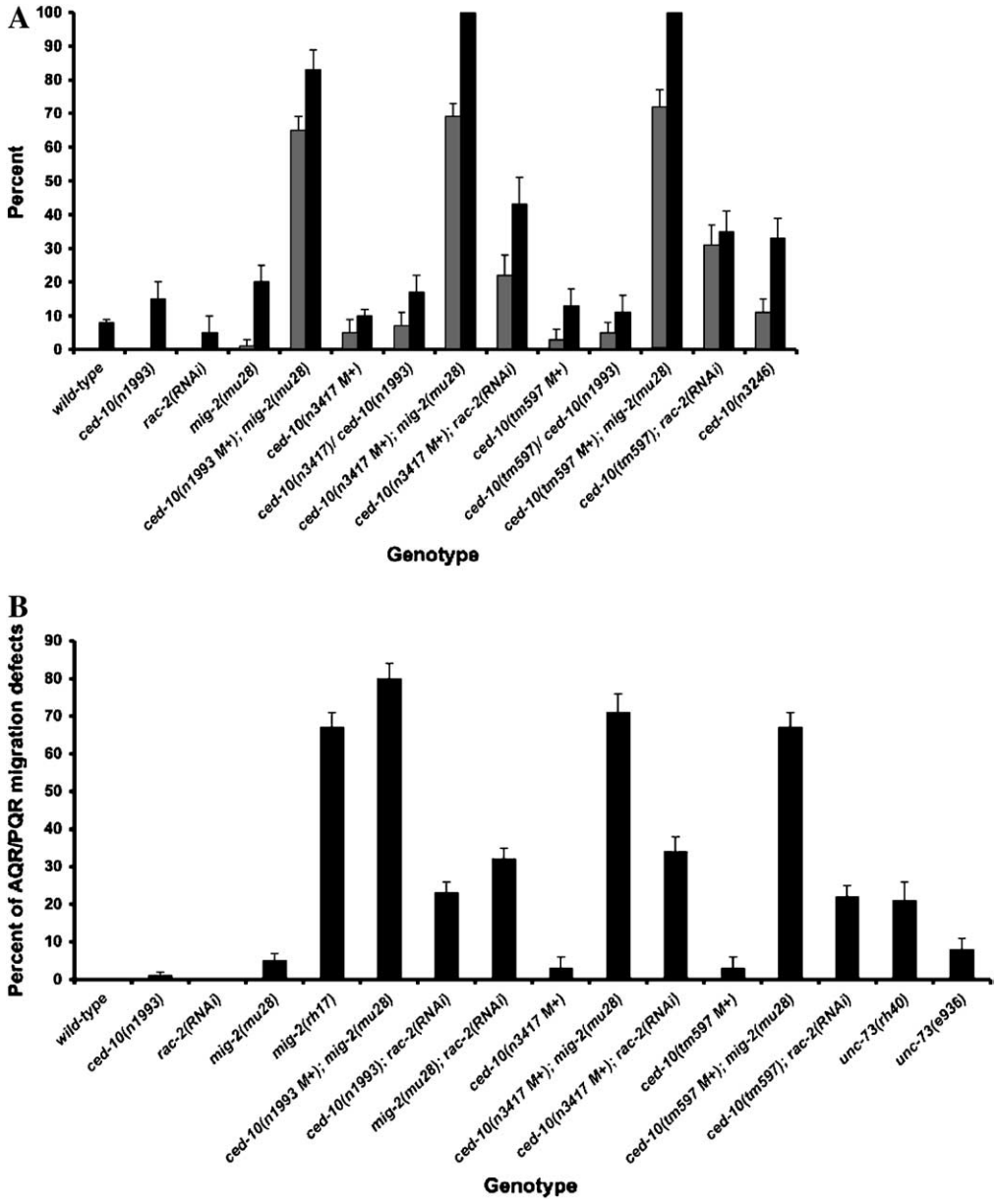

FIGURE 3.—Null *ced-10* alleles synergize with *mig-2* and *rac-2* in axon pathfinding and neuronal migration. (A) The graph displays the percentage of axon pathfinding defects (*y*-axis) of various genotypes (*x*-axis). Shaded bars represent PDE axon guidance defects and solid bars represent VD/DD axon pathfinding defects (see MATERIALS AND METHODS). M+ indicates that the mutants had wild-type maternal contribution for that locus. (B) The graph displays the percentage of AQR and PQR neuronal migration defects along their normal routes (*y*-axis) in various genotypes (*x*-axis). See MATERIALS AND METHODS for scoring of AQR and PQR migration defects along their normal routes. M+ indicates that the mutants had wild-type maternal contribution for that locus. In all cases except *mig-2(rh17)*, AQR and PQR were equally affected. In *mig-2(rh17)* mutants, PQR was predominantly affected. Error bars represent the standard error of the proportion.

3B). While PQR was more often affected than AQR in *mig-2(rh17)* animals, defects in AQR migration were also observed.

Previous studies implicated the Dbl-homology GTP exchange factor (DH-GEF) UNC-73 Trio as acting in all three Rac pathways in PDE axon pathfinding and CAN cell migration (LUNDQUIST *et al.* 2001; WU *et al.* 2002). Furthermore, *unc-73* mutations affect the ability of Q cells to polarize and the ability of Q cells and their descendants to execute migrations. However, *unc-73* does not affect orientation of Q-cell polarity as do *unc-40*, *dpy-19*, and *mab-5* (*i.e.*, *unc-73* mutants do not display QL direction of migration defects) (HONIGBERG and KENYON 2000). Consistent with these results, we found that *unc-73* mutants displayed defects in AQR and PQR migration along their normal routes (Figure 3B) but did not affect PQR direction of migration. These data indicate that the Racs and UNC-73 control the ability of Q cells or descendants to migrate along their normal routes. No defects in direction of PQR migration were observed, suggesting that UNC-73 and the Racs are not involved in controlling the direction of PQR migration. The *unc-73(rh40)* allele specifically eliminates the Rac GEF activity of UNC-73. The severity of the defects of *unc-73(rh40)* were less than those of *mig-2; ced-10* double mutants, indicating that UNC-73 might not be the only Rac GEF involved in the migrations of Q cells or their descendants.

MIG-15 NIK controls axon pathfinding: Vertebrate NIK (SU *et al.* 1997) and Drosophila Misshapen (TREISMAN *et al.* 1997) are serine/threonine kinases of the GCK family and contain an N-terminal STE20-like kinase domain and a C-terminal CNH (citron/NIK homology) domain, which is thought to interact with

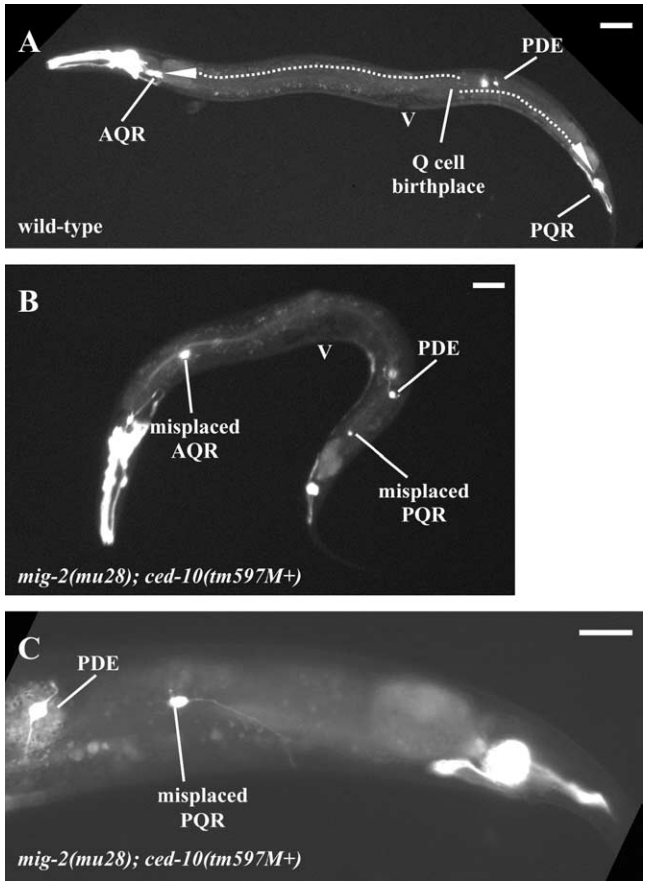

Figure 4.—AQR and PQR neuronal migration defects in *rac* double mutants. Anterior is to the left and dorsal is up. All are fluorescence micrographs of fourth larval stage (L4) animals with *osm-6::gfp* expression in the AQR, PQR, and other neurons. The position of the vulva is indicated by a "V." (A) A wild-type animal. The position of the birthplace of QL and QR is indicated, as are the migration routes of QL and descendants (PQR) (posterior arrow) and QR and descendants (AQR) (anterior arrow). The final positions of PQR and AQR are indicated. (B) A *ced-10(tm597M+); mig-2(mu28)* animal with mispositioned AQR and PQR neurons. The neurons failed to complete their migrations along their normal paths (AQR migrated anteriorly and PQR migrated posteriorly, but both failed to reach their normal positions). (C) The posterior region of *ced-10(tm597M+); mig-2(mu28)* animal with a mispositioned PQR neuron on the left side of the animal. Bars: A and B, 20 μm; C, 10 μm.

Rho-family GTPases. In *C. elegans*, the *mig-15* gene encodes a NIK homolog (Figure 5A) (Poinat *et al.* 2002), and RNAi of *ced-10, rac-2*, and *mig-2* increase the frequency of axon pathfinding defects in the VD/DD commissural axons of a hypomorphic *mig-15* mutation (Poinat *et al.* 2002), suggesting that *mig-15* and the *rac* genes interact in axon pathfinding, although it is unclear if they act in the same pathway or in parallel pathways.

To understand the relationship of MIG-15 NIK and Rac signaling in PDE axon pathfinding, we first analyzed the effects of *mig-15* mutants on PDE axon development. Alone, *mig-15(rh148)* and *mig-15(rh80)* displayed moderate defects in PDE axon pathfinding, including ventral PDE axon guidance errors (25% and 64%, respectively; Figures 5B and 6A) and formation of ectopic neurites (Figure 6A). We were unable to maintain the *mig-15(rh326)* allele as a homozygous strain due to sterility and larval lethality caused by the mutation. However, *mig-15(rh326)* homozygotes from a *mig-15(rh326)/+* heterozygous mother (wild-type *mig-15* maternal contribution) displayed 62% PDE ventral axon pathfinding errors, compared to 23% for *mig-15(rh80)* animals with wild-type maternal contribution (Figure 5B).

On the basis of PDE axon defects (Figure 5B) and on viability and growth, the three *mig-15* alleles formed an allelic series from least severe to most severe: *rh148* < *rh80* < *rh326*. We determined the molecular nature of the three *mig-15* alleles. The weakest allele, *rh148*, resulted in a missense change of valine 169 to glutamic acid (V169E) (Figure 5A). On the basis of comparison with the crystal structures of other GCK kinase family members, V169 of MIG-15 might contribute to the hydrophobic ATP binding pocket of the putative kinase domain (Figure 5A) (Lowe *et al.* 1997; Niefind *et al.* 1998; Marchler-Bauer *et al.* 2005). In *rh148*, a charged glutamic acid residue at this position might interfere with ATP binding and affect the activity of the kinase. *rh80* resulted in a nonsense change of tryptophan 898 to an opal stop codon (W898STOP) (Figure 5A) in the middle of the conserved CNH domain coding region, which is thought to mediate interaction with Rho and Rac GTPases (Madaule *et al.* 1995; Marchler-Bauer *et al.* 2005). *rh326* resulted in a nonsense change of glutamine 439 to an ochre stop codon (Q439STOP) (Figure 5A). *rh326* is a good candidate for a *mig-15* null mutation, as *rh326* resulted in an early predicted stop and had the strongest PDE axon pathfinding defects. Both *rh148* and *rh80* likely retain some *mig-15* activity.

MIG-15 acts with the Racs in axon pathfinding: The PDE axon pathfinding defects of hypomorphic *mig-15(rh148)* were enhanced by *ced-10(n1993)*. For example, *mig-15(rh148)* displayed 25% PDE ventral guidance errors, whereas *mig-15(rh148); ced-10(n1993)* doubles displayed 69% (Figure 5B). Double mutants of *ced-10* with *mig-15(rh148)* were viable and fertile, whereas *ced-10(n1993)* double mutants with *mig-15(rh80)* and *mig-15(rh326)* arrested as larvae. Despite wild-type maternal *mig-15* (indicated by M+ in the genotype), double mutants of *ced-10(n1993); mig-15(rh80M+)* displayed 63% PDE ventral axon guidance errors compared to 23% for *mig-15(rh80M+)* alone (Figure 5B). *ced-10(n1993); mig-15(rh326M+)* displayed 74% PDE axon pathfinding defects compared to 62% for *mig-15(rh326M+)* alone (Figure 5B), suggesting that *ced-10(n1993)* might slightly enhance *mig-15(rh326)*. However, *ced-10(n1993); mig-15(rh326M+)* doubles were often larval lethal and had severe body morphology defects that might have contributed to apparent PDE axon defects. *mig-2(mu28)*

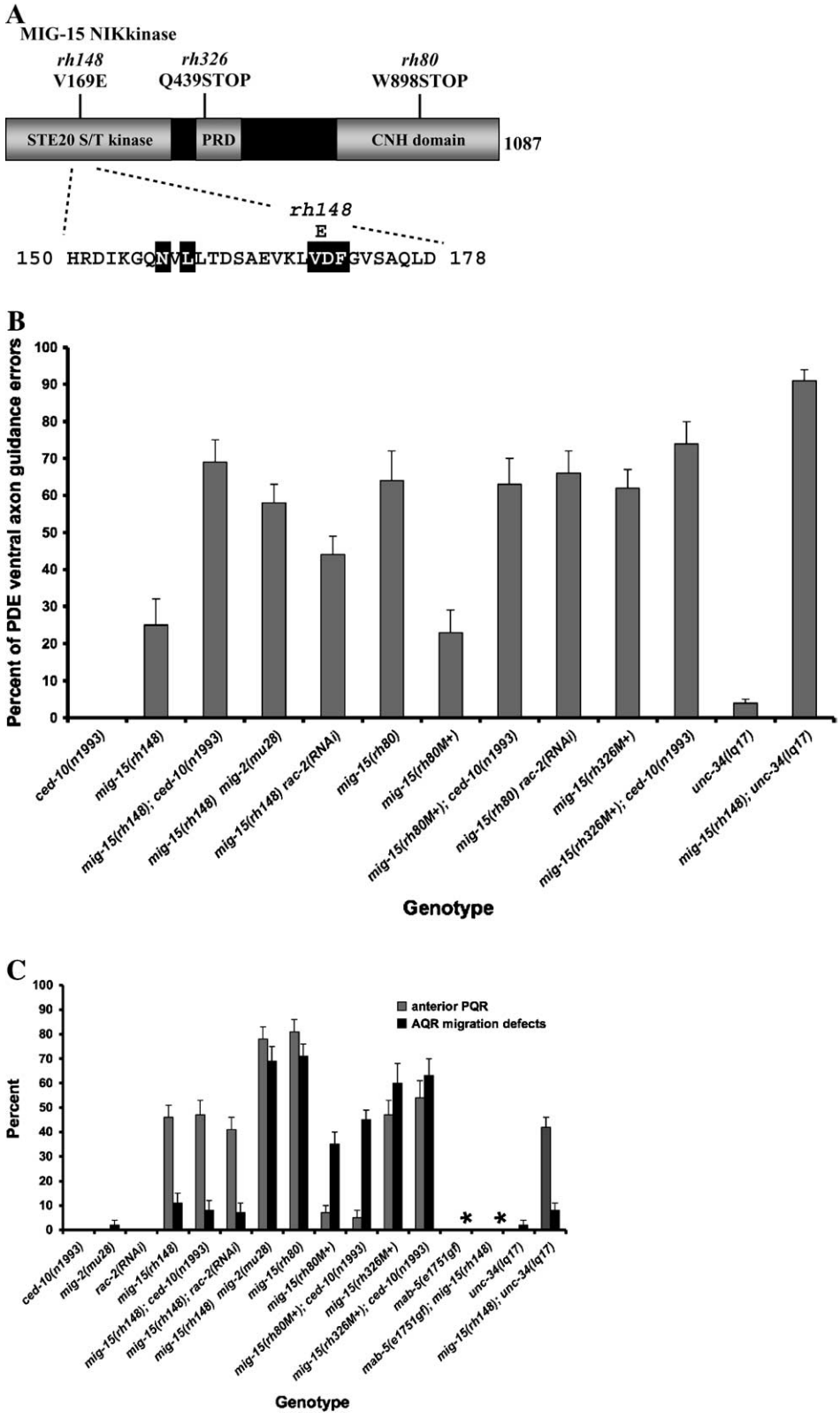

FIGURE 5.—Effects of *mig-15* and *rac* mutants on PDE axon pathfinding and AQR/PQR migration. (A) A diagram of the predicted 1087-residue MIG-15 polypeptide (N terminus to the left) (GenBank accession no. AF087131; Wormbase Gene Model ZC504.4a). The N terminus of the polypeptide contains a region similar to a serine-threonine kinase of the STE20 class (STE20 S/T kinase), and the C-terminus contains a region similar to a regulatory domain of the protein Citron (CNH). The central region of the polypeptide contains a proline-rich domain (PRD). The locations of the *mig-15* alleles are shown above the structure. Below the structure is the polypeptide sequence in the region of the *rh148* lesion. Residues in this region that contribute to the ATP binding pocket of the kinase domain are boxed (residues outside of this region also contribute to the ATP binding pocket). *rh148* was a T-to-A transversion at position 503 in the *mig-15* open reading frame resulting in a V169E missense mutation; *rh80* was a G-to-A transition at position 2694 in the *mig-15* open reading frame resulting in an opal stop (TGG to TGA); and *rh326* was a G-to-A transition at position 1315 in the *mig-15* open reading frame resulting in an ochre stop (CAA to TAA). (B) The graph depicts the percentage of PDE axon guidance defects (*y*-axis) in various genotypes (*x*-axis) (see MATERIALS AND METHODS for PDE scoring). (C) The graph represents percentages of defects (*y*-axis) in various genotypes (*x*-axis). Gray bars represent the percentage of anteriorly displaced PQR neurons (anterior to the vulva), indicating a defect in the direction of PQR migration. Black bars represent the percentage of AQR neurons that migrated anteriorly but failed to reach their normal final position. M+ indicates that the mutants had wild-type maternal contribution for that locus. The asterisks (*) denote that in *mab-5(e1751)* and *mig-15(rh148); mab-5(e1751)* animals, AQR is misdirected posteriorly and resides among the phasmid neurons 86% and 73% of mutants, respectively (see RESULTS). Error bars represent the standard error of the proportion.

also enhanced the PDE axon defects of hypomorphic *mig-15(rh148)* to a level similar to *mig-15(rh80)* and *mig-15(rh326M+)*, and *rac-2(RNAi)* slightly enhanced *mig-15(rh148)* but had no effect on *mig-15(rh80)*.

Both *ced-10* and *mig-2* mutations enhanced the PDE axon defects of the weak *mig-15(rh148)* allele to levels similar to the stronger *mig-15(rh80* and *rh326)* alleles, and *ced-10* enhanced the defects *of mig-15(rh80)* with

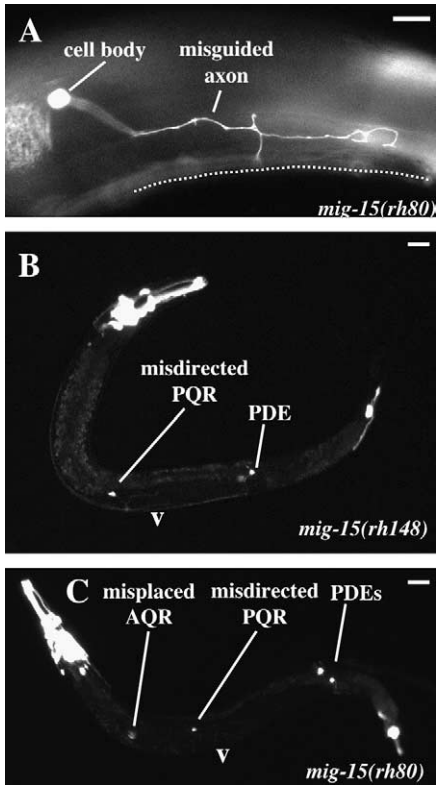

Figure 6.—PDE axon pathfinding and AQR/PQR cell migration defects in *mig-15* mutants. Anterior is to the left and dorsal is up. All are fluorescence micrographs of fourth larval stage (L4) animals with *osm-6::gfp* expression in the PDEs, AQR, PQR, and other neurons. The position of the vulva is indicated by a "V." (A) A PDE axon of a *mig-2(rh80)* animal failed to extend directly to the ventral surface (dashed line) and instead wandered laterally. The axon also exhibited ectopic neurites. (B) A left-lateral view of a *mig-15(rh148)* animal. The PQR neuron migrated anteriorly instead of posteriorly. (C) A left-lateral view of a *mig-15(rh80)* mutant. The PQR neuron migrated anteriorly, and the AQR neuron did not complete its anterior migration. Bars: A, 10 μm; B and C, 20 μm.

wild-type maternal *mig-15* contribution, suggesting that both *rh148* and *rh80* are hypomorphic alleles. No defects in *rac; mig-15* doubles were strikingly stronger than the putative null allele *mig-15(rh326M+)* alone. These data are consistent with a model in which *mig-15* and the three *rac* genes might participate in the same pathway (*i.e.*, the three Racs have overlapping roles but *mig-15* might act in each Rac pathway). However, *ced-10 (n1993)* might have slightly enhanced the *mig-15(rh326)* null allele, raising the possibility that *mig-15* and *ced-10* act in parallel pathways. In any case, these data indicate that *mig-15* and three *rac* genes *ced-10*, *mig-2*, and *rac-2* act together to control PDE axon pathfinding.

MIG-15 NIK and MIG-2 Rac control direction of PQR migration: We found that *mig-15* mutants alone affected the direction of PQR migration. In 46% of *mig-15(rh148)*, 81% of *mig-15(rh80)*, and 47% of *mig-15(rh326M+)* animals, PQR was positioned anterior to the vulva, indicating that PQR, its precursors from QL, or QL itself migrated anteriorly rather than posteriorly (Figure 5C and Figure 6, B and C). *mig-15(rh326M+)* was weaker than *mig-15(rh80)*, possibly because of wild-type maternal *mig-15* activity. Indeed, *rh80* with maternal *mig-15(+)* was weaker than *mig-15(rh326M+)* (Figure 5C). *mig-15* mutants also displayed defects in AQR migration along its normal route (11%, 71%, and 60% in *rh148*, *rh80*, and *rh326M+* respectively; Figure 5C and Figure 6C).

AQR/PQR defects of *mig-15* mutants were not affected by *ced-10(n1993)* or by *rac-2(RNAi)* (Figure 5C). In contrast, the *mig-2(mu28)* mutation significantly enhanced the PQR directional migration defects and the AQR migration defects of *mig-15(rh148)* to a level similar to that of *mig-15(rh80)* alone (Figure 5C). Alone, *mig-2(mu28)* had no effect on directional PQR migration, but did display weak defects in AQR and PQR migration along their normal routes (5%; Figure 3B). These data indicate that MIG-2 might act in the MIG-15 pathway in controlling direction of PQR migration, and that CED-10 and RAC-2 are not involved in this process. The AQR migration defects of *mig-15* were also enhanced by *mig-2(mu28)* but not by *ced-10(n1993)* or *rac-2(RNAi)*. Constitutively active *mig-2(rh17)*, which affected the ability of AQR and PQR to migrate along their normal routes (Figure 3B), did not affect AQR or PQR direction of migration (data not shown).

MIG-15 might act upstream of MAB-5 in controlling PQR direction of migration: Our data indicate that *mig-15* controls the direction of PQR migration, which could be due to defects in the polarity of QL cell or its daughters. Q-cell polarity occurs in at least two phases: an initial morphological polarity and short migration, where QL polarizes to the posterior and QR polarizes to the anterior; and a later Wnt signal that instructs posterior migration of QL and daughters but not QR and daughters (Honigberg and Kenyon 2000). Genes known to control initial QL polarity include *unc-40* and *dpy-19* (Honigberg and Kenyon 2000). We found that the PQR neuron was misdirected anteriorly in 25% of *unc-40(e271)* mutants ($n = 100$) and 33% of *dpy-19(e1259)* mutants ($n = 100$). The misdirected PQR neurons in these mutants migrated anteriorly to a position near the normal final anterior position of AQR (a complete anterior migration). In contrast, the migration of the misdirected PQR neurons in *mig-15* often failed along their anterior routes (Figure 6, B and C). Mutations in Wnt signaling genes also cause incomplete migrations of misdirected QL daughters (Whangbo and Kenyon 1999; Honigberg and Kenyon 2000; Herman 2001).

After the initial polar posterior migration of QL that is dependent upon UNC-40 and DPY-19, Wnt signaling induces the expression of the homeodomain transcription factor MAB-5 in QL but not in QR (Salser and Kenyon 1992; Whangbo and Kenyon 1999; Honigberg

and KENYON 2000). MAB-5 expression in QL and daughters controls these cells' further posterior migrations. As expected, the QL daughter PQR was misplaced anteriorly in 75% ($n = 100$) of *mab-5(e1239)* loss-of-function mutants. The misdirected PQR neurons reached the normal anterior position of AQR, similar to *dpy-19* and *unc-40* mutants. The gain-of-function *mab-5(e1751)* allele causes constitutive *mab-5* activity in both QL and QR and daughter cells independent of Wnt signaling (SALSER and KENYON 1992). As expected, PQR placement was normal (in the posterior) in all *mab-5(e1751gf)* animals examined ($n = 100$) (Figure 5C) and AQR was mispositioned in the posterior among the phasmid neurons in 86% ($n = 100$) of *mab-5(e1751gf)* animals.

These data show that PQR was mispositioned anteriorly in *mig-15* mutants and was normally positioned in *mab-5(e1751gf)* mutants. In *mig-15(rh148); mab-5(e1751gf)* double mutants, AQR and PQR placement resembled that of *mab-5(e1751)* alone: PQR was positioned normally in the posterior in all *mig-15(rh148); mab-5(e1751gf)* animals examined ($n = 100$) (Figure 5C) and AQR was found in the posterior among the phasmid neurons in 73% ($n = 100$) of double mutants. This result indicates that *mab-5* activation in QL compensated for loss of *mig-15* and that *mig-15* might act upstream of *mab-5* in PQR migration.

***mig-2(lq13), ced-10(n1993lq20),* and *ced-10(n3246)* are gain-of-function *rac* mutations:** To identify other genes that act redundantly with *ced-10* in axon pathfinding, we undertook a genetic screen for mutations that were synthetic lethal with *ced-10* with the idea that the genes identified by these mutations might also act in parallel to *ced-10* in axon pathfinding (see MATERIALS AND METHODS for details of the screen).

The *lq13* mutation was a new allele of *mig-2* and *lq20* was a new allele of *ced-10* (see MATERIALS AND METHODS). *ced-10(n1993); mig-2(lq13)* double mutants arrested as embryos and larvae with defects in gastrulation, similar to *ced-10* null animals and *ced-10(n1993); mig-2(mu28)* animals (data not shown). *ced-10(n1993lq20)* mutants displayed variable lethality characteristic of other *ced-10*-related lethality (defects in gastrulation; data not shown). However, *n1993lq20* also gave rise to nonlethal "escaper" animals that were severely Unc. We found that *lq13* was a C-to-T change that results in a missense mutation of serine 75 of MIG-2 to phenylalanine (S75F) (Figure 1B), and that *lq20* was a C-to-T missense mutation resulting in a proline 29-to-leucine change (P29L) in CED-10 (Figure 1C). We also confirmed the presence of the *n1993* lesion in this strain (a G-to-T transition resulting in a change of valine 190 to glycine). *ced-10(n1993)* is a hypomorphic allele that retains some *ced-10* activity. Because *n1993* is not a null allele, the potential gain-of-function effect of *lq20* could be expressed in the *n1993* background.

In contrast to *mig-2* and *ced-10* null mutants, *mig-2(lq13)* animals were slightly uncoordinated and *ced-10(n1993lq20)* were severely uncoordinated (data not shown). Furthermore, *mig-2(lq13)* and *ced-10(n1993lq20)* mutants displayed PDE axon pathfinding defects not observed in *mig-2* or *ced-10* loss-of-function mutants (Figure 7A): the *mig-2(mu28)* null mutant displayed 1% PDE axon guidance errors whereas *mig-2(lq13)* displayed

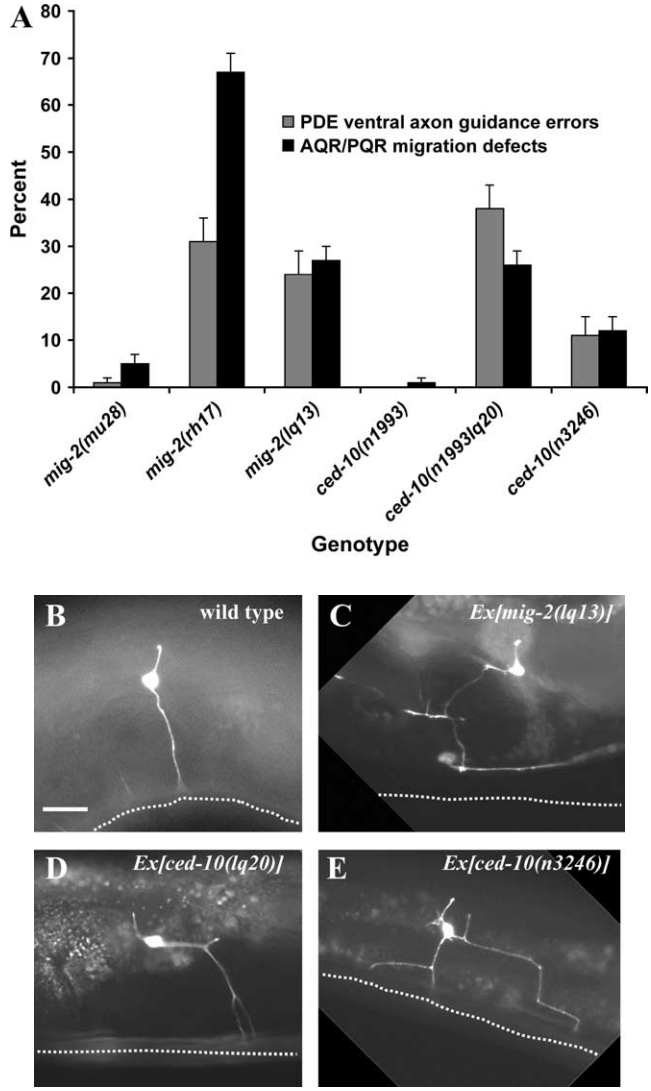

FIGURE 7.—PDE axon pathfinding defects and AQR/PQR migration defects in *rac* gain-of-function mutants. (A) The graph represents the percentage of defects (*y*-axis) in various genotypes (*x*-axis). Gray bars represent the percentage of PDE axon guidance defects, and the black bars represent percentages of AQR and PQR migration defects along their normal routes (see MATERIALS AND METHODS for scoring). In each genotype, PQR was affected more often than AQR. Error bars represent the standard error of the proportion. (B–E) Fluorescence micrographs of *osm-6::gfp* expression in PDE neurons in animals harboring gain-of-function *rac* transgenes (see MATERIALS AND METHODS). Anterior is to the left and dorsal is up. The dashed line indicates the ventral midline. (B) The wild-type PDE axon extends directly to the ventral midline. (C–E) The axons of animals transgenic for *mig-2(lq13)*, *ced-10(lq20)*, and *ced-10(n3246)* were misguided and displayed ectopic neurites. Bar for B–E, 10 μm.

24%; and *ced-10(n3417* and *tm597)* null mutants displayed 3–5% PDE axon defects compared 38% in *ced-10 (n1993lq20)*. The previously described mutation *ced-10 (n3246)* is a G-to-A transition resulting in a change of glycine 60 of CED-10 to arginine (G60R) (Figure 1C) (Reddien and Horvitz 2000). *ced-10(n3246)* animals also displayed slight uncoordination (data not shown) as well as defects in PDE and VD/DD axon pathfinding (Figures 3A and 7A) not observed in *ced-10* null mutants.

mig-2(lq13), *ced-10(n1993lq20)*, and *ced-10(n3246)* affected migration of AQR and PQR neurons along their normal routes (Figure 7A) [*e.g.*, 5% for *mig-2(mu28)* compared to 27% for *mig-2(lq13)*]. While execution of AQR and PQR migration was affected, these mutations had no effect on direction of AQR or PQR migration (data not shown). Together, these data indicate that *mig-2(lq13)*, *ced-10(n1993lq20)*, and *ced-10(n3246)* are not simple loss-of-function mutations and are likely to be gain-of-function mutations. However, each of these mutations was recessive to wild-type for Unc and for PDE axon defects and AQR/PQR migration (data not shown).

To further test the idea that *lq13*, *n1993lq20*, and *n3246* were gain-of-function mutations, we used a transgenic assay to study the consequences of expression of MIG-2 with the *lq13* mutation and CED-10 with the *lq20* and *n3246* mutations specifically in the PDE neuron. We constructed transgenes consisting of the *mig-2* or *ced-10* genomic coding regions (exons and introns; Struckhoff and Lundquist 2003) downstream of the *osm-6* promoter, which is expressed in all ciliated sensory neurons including PDE (see materials and methods). Consistent with previous results (Struckhoff and Lundquist 2003), we found that transgenic expression of wild-type MIG-2 or CED-10 in the PDE caused few defects in axon pathfinding or PDE morphogenesis (data not shown). In contrast, transgenic expression of MIG-2(lq13), CED-10(lq20), and CED-10(n3246) caused severe defects in PDE axon pathfinding: the PDE neurons displayed ectopic neurites and misguided axons (Figure 7C) similar to the phenotype of *mig-2(mu28); ced-10(n1993)* loss-of-function mutants. However, MIG-2(lq13), CED-10(lq20), and CED-10(n3246) expression did not result in robust formation of ectopic lamellipodia-like and filopodia-like structures caused by transgenic expression of constitutively active MIG-2(G16V) or CED-10(G12V) (Struckhoff and Lundquist 2003).

In summary, these data suggest that *mig-2(lq13)*, *ced-10(n1993lq20)*, and *ced-10(n3246)* are gain-of-function alleles: in contrast to the null alleles of *mig-2* and *ced-10*, each caused axon pathfinding and cell migration defects; and transgenic expression of these mutant molecules caused dominant PDE axon defects whereas transgenic expression of wild-type CED-10 and MIG-2 did not.

***unc-34(lq17)* affects splicing of the *unc-34* transcript:** The *ced-10* synthetic lethal mutation *lq17* was found to be a hypomorphic allele of *unc-34*, which encodes the *C. elegans* homolog of the cytoskeletal signaling protein Enabled (Figure 8A) (Withee *et al.* 2004). *ced-10(n1993); unc-34(lq17)* animals that lost the *ced-10(+)* array were embryonic lethal with a Gex phenotype similar to *ced-10* null mutants (data not shown). Thus, UNC-34 Enabled might act redundantly with Rac signaling in gastrulation.

On the basis of the synthetic lethality with *ced-10(n1993)*, we determined that the genetic position of *lq17* was on the left arm of linkage group V (see materials and methods), the location of the *unc-34* gene that has previously been shown to affect axon pathfinding and neuronal migration. We found that *lq17* failed to complement the Unc phenotype of three *unc-34* alleles, *e315*, *gm104*, and, *e951*, suggesting that *lq17* was an allele of *unc-34* (data not shown). We determined the nucleotide sequence of *unc-34* from *lq17* mutants and found a G-to-A transition that affected the first nucleotide residue of the last *unc-34* intron and that was predicted to abolish use of this site as a splice donor (Figure 8B). To determine the effect of the *lq17* mutation on the *unc-34* transcript, we used RT–PCR to generate cDNAs representing the *unc-34* transcript from *lq17* mutants. In wild type, we observed the expected cDNA product of approximately 1.4 kb, and sequencing confirmed that this product represented the *unc-34/Y50D4C.1a* mRNA. Using the same RT–PCR protocol, we obtained a cDNA of approximately 1.4 kb from *unc-34(lq17)* animals. Sequencing of the 1.4-kb *lq17* transcript revealed that a cryptic donor splice site 14 nt to the 3′ of the normal intron 5′ splice donor site was used in this transcript, resulting in a 13-bp insertion into the *unc-34* transcript (Figure 8, B and C). The 13-bp addition introduced an in-frame stop codon that would result in truncation of the C-terminal 43 residues of the UNC-34 polypeptide.

The C-terminus of UNC-34 contains a predicted EVH2 domain (Figure 8A), which consists of A, B, and C functional subdomains (Krause *et al.* 2003; Withee *et al.* 2004). The *lq17* mutation leads to a 43-residue truncation of the UNC-34 polypeptide that is predicted to remove most of the EVH2 C domain while leaving other domains unaffected (Figure 8C). The EVH2 C domain is thought to mediate tetramerization of the Enabled molecule, which facilitates its actin-binding ability (Haffner *et al.* 1995; Bachmann *et al.* 1999; Zimmermann *et al.* 2002). Thus, an UNC-34 polypeptide produced in *lq17* animals might lack the ability to tetramerize but might retain other functions of the molecule.

UNC-34 Ena acts in parallel to CED-10 Rac, RAC-2 Rac, and MIG-2 Rac in axon pathfinding and neuronal migration: To assess the effect of the new *lq17* mutation on these processes, we isolated *lq17* away from *ced-10(n1993)* and the *ced-10(+)* array and scored PDE axon pathfinding and AQR/PQR migration in these animals. Alone, *lq17* animals were slightly Unc but less severely so than extant null *unc-34* alleles (data not shown).

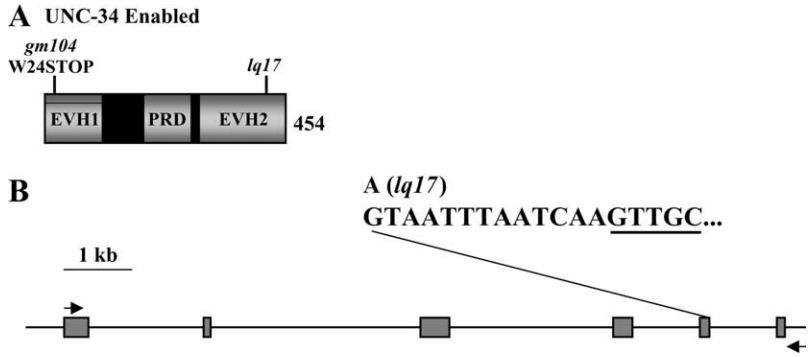

C

```
1/1                                         31/11
ATG ACC TAC AAC GAA TCG ACA AAA GGA TGG GTA CTA CTC GGC GGA AAT GAT GAT TCA ATG
M   T   Y   N   E   S   T   K   G   W   V   L   L   G   G   N   D   D   S   M
61/21                                       91/31
ACA AAT GTT CGC CTA ATC CAA GAC ATT CGG CGA CCC GAG TTT CGG ATT GTA TCC AAC CGC
T   N   V   R   L   I   Q   D   I   R   R   P   E   F   R   I   V   S   N   R
121/41                                      151/51
GCT GAC AGC ACG AAT ATC TTG AAT TGT AAT ATT TAT CGA GGA ATC AAA TAT CAC AAG GCC
A   D   S   T   N   I   L   N   C   N   I   Y   R   G   I   K   Y   H   K   A
181/61                                      211/71
ACA CCA ATG TTT CAT CAA TGG CGT ACC GAA CAG CGG CGG GTG TAT GGG CTG AAT TTC GAG
T   P   M   F   H   Q   W   R   T   E   Q   R   R   V   Y   G   L   N   F   E
241/81                                      271/91
AAT GAA CAG GAT GCG ACA ATG TTT TTA AGC ATT GTG TTA CAG GCG ATT GAG ACG TTG AAA
N   E   Q   D   A   T   M   F   L   S   I   V   L   Q   A   I   E   T   L   K
301/101                                     331/111
GTT CAT GAT ATG AAT GGA ATT AGT GAT TAT CAA CAG ATG CAT CAA GTC GAC AAT GTC TAT
V   H   D   M   N   G   I   S   D   Y   Q   Q   M   H   Q   V   D   N   V   Y
361/121                                     391/131
CAG GAT CCC CAC CAG CAC CTA ATG CAC ATT CAC TCG GCG CCG AAT TTT CAC GAT GAG AAT
Q   D   P   H   Q   H   L   M   H   I   H   S   A   P   N   F   H   D   E   N
421/141                                     451/151
CAG AAT GCC GCG AAT TTT CGA AAA ACG TCC CAA CAC GCC TCG AGC CTC CTC TCC AGT ACT
Q   N   A   A   N   F   R   K   T   S   Q   H   A   S   S   L   L   S   S   T
481/161                                     511/171
GCA GCA GCA CTA ACA CAA CAA CAA CGT CGA GCC TCT CAA AGT TCA AGT ACA AGT GCC GGA
A   A   A   L   T   Q   Q   Q   R   R   A   S   Q   S   S   S   T   S   A   G
541/181                                     571/191
TCT TCA ATT CCC CAT GCT CCA CCA CCA CCA GTT CCA CTT ACC AGT AAC ATT CCA CAG GCT
s   S   I   P   H   A   P   P   P   P   V   P   L   T   S   N   I   P   Q   A
601/201                                     631/211
CCA CCA GCT CCA CCT CCT CCA ATC GGT GGT ATT GCT CCG GTA AAT GCT CAC GGA GCT CCA
P   P   A   P   P   P   P   I   G   G   I   A   P   V   N   A   H   G   A   P
661/221                                     691/231
CCA CCA CCA CCA CTT CCT CCA GTT GGT GCA GGT GCT CCA CCG CCA CCT CCG CCA CCT CCA
P   P   P   P   L   P   P   V   G   A   G   A   P   P   P   P   P   P   P   P
721/241                                     751/251
CCG CCA GCA CAG TTG ATG GCC TCC AGT GGA ACG CCG AGT CTC GCA GAA CAG CTG AAA ATG
P   P   A   Q   L   M   A   S   S   G   T   P   S   L   A   E   Q   L   K   M
781/261                                     811/271
AGA AGT CAG CAG GGC CTG AAA GCG ACG AGT AAT GGG GTT AAA GCT GCC GCT GCA GAG CCC
R   S   Q   Q   G   L   K   A   T   S   N   G   V   K   A   A   A   A   E   P
841/281                                     871/291
GAG AAG CCT GCT GCG AAA GGA GCC GGC AAT CTA ATG TCC GAA TTG GAG GCT CAA CTA AAT
E   K   P   A   A   K   G   A   G   N   L   M   S   E   L   E   A   Q   L   N
901/301                                     931/311
AAG CGA AAA ATG ACA CAA GCG AAA TCG GAT GCA GTT GAT TCG AAA TCA AAT ACG AGC AAT
K   R   K   M   T   Q   A   K   S   D   A   V   D   S   K   S   N   T   S   N
961/321                                     991/331
GGA TCA TCG GAT AGC GGA TGT GGT ACG GCG ACG TCG ACG AAT GGA TGT GGA TCA TCG AAT
G   S   S   D   S   G   C   G   T   A   T   S   T   N   G   C   G   S   S   N
1021/341                                    1051/351
GGT GGA TCG GTT GGA TCG GCG GCC GCC AAA AAA TGG TCT GTT TCA GAT GCA ACG AAG CCC
G   G   S   V   G   S   A   A   A   K   K   W   S   V   S   D   A   T   K   P
1081/361                                    1111/371
ATG GAT AGT CCG AAG ACG CAT AGA AAA CTT CCA TCC GCC TCA TCA CTA TTC TCA CAA GAA
M   D   S   P   K   T   H   R   K   L   P   S   A   S   S   L   F   S   Q   E
1141/381                                    1171/391
GAT TCA TCA TCA TCA TCA TCA TCT ACG CTG ACA CCT TCA AAA CCA ACA ACA AAT GGA ACG
D   S   S   S   S   S   S   S   T   L   T   P   S   K   P   T   T   N   G   T
1201/401                                    1231/411
TCA TCG GCG ATT CCG AAT GAT CTA CTC GAG AG a taa ttt aat caa  A CTC CGC GCT GAC
S   S   A   I   P   N   D   L   L   E   R   *                   L   R   A   D
                    1261/421                                1291/431
ATA ATG GTC GAA ATG CGA CTG GAG ATG AAC AAG CTC GAG CAA CGA ATC GTC GAG GCC AAC
I   M   V   E   M   R   L   E   M   N   K   L   E   Q   R   I   V   E   A   N
                    1321/441                                1351/451
GAT CGG GCC GTC GAT CGG GCC GTC GAG ACT ATT TTG AAC GCG ATT GGT GGC CGT CGA TAG
D   R   A   V   D   R   A   V   E   T   I   L   N   A   I   G   G   R   R   *
```

FIGURE 8.—The *unc-34(lq17)* mutation affects splicing of the *unc-34* transcript. (A) A schematic of the 454-residue UNC-34 polypeptide (GenBank accession no. NP_503360), which contains an N-terminal EVH1 domain, a proline-rich domain (PRD), and a C-terminal EVH2 domain. The locations of the *gm104* (WITHEE *et al.* 2004) and *lq17* lesions are indicated. (B) The structure of the *unc-34* locus. Shaded boxes represent exons. 5′ is to the left. The arrows represent the positions of the primers used to generate *unc-34* cDNAs by RT–PCR. The sequence of the 5′ of the last *unc-34* intron is shown above the gene structure. The *lq17* mutation is indicated (a G-to-A transition of the first nucleotide of the intron), and the cryptic splice site used in *unc-34(lq17)* mutants is underlined. (C) The sequence of the *unc-34(lq17)* cDNA generated by RT–PCR. The nucleotide sequence and conceptual translation are shown. Numbering represents nucleotide/amino acid residue. Block C of the EVH2 domain is underlined. The 13-nucleotide insertion due to use of a cryptic splice site in *unc-34(lq17)* is shown in lower-case letters. The insertion results in a premature in frame stop codon, which truncates block C of the EVH2 domain.

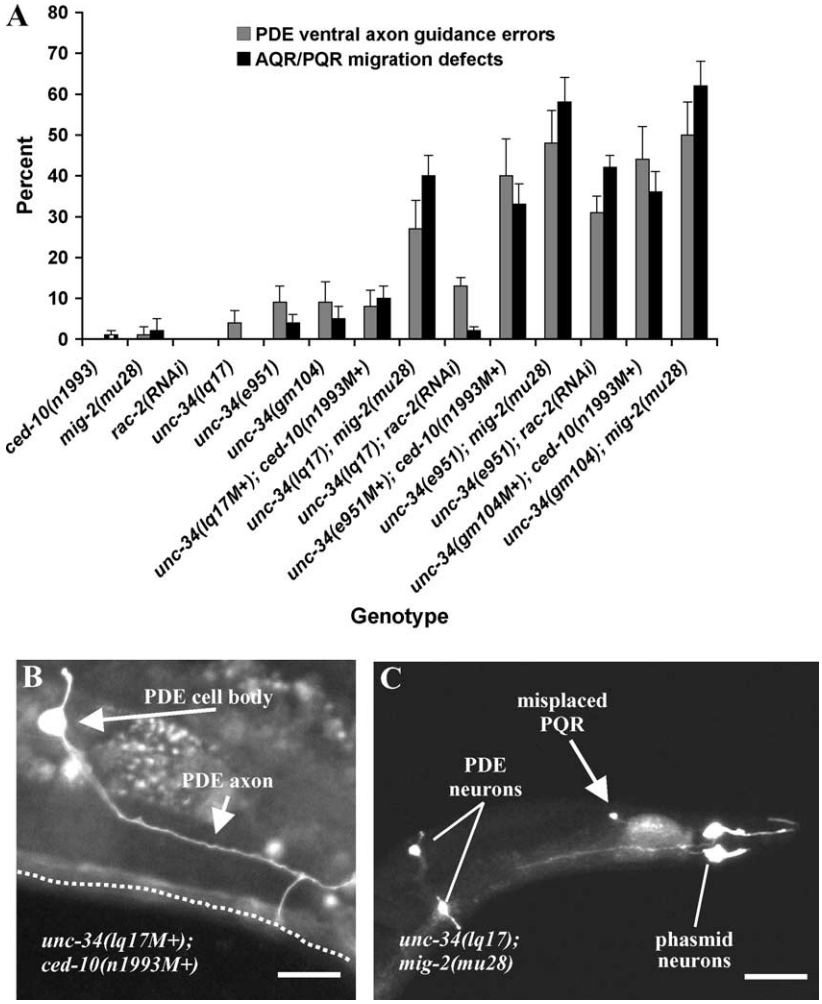

FIGURE 9.—PDE axon pathfinding and AQR/PQR migration defects in *unc-34* mutants. (A) The graph represents percentages of defects (*y*-axis) in various genotypes (*x*-axis). Shaded bars represent PDE ventral axon guidance errors, and solid bars represent AQR/PQR migration defects along their normal routes. M+ indicates that the animals had wild-type maternal contribution for that locus. Error bars represent the standard error of the proportion. (B and C) Fluorescent micrographs of animals with *osm-6::gfp* expression. (B) A *unc-34(lq17M+); ced-10(n1993M+)* animal had a misguided PDE axon that failed to extend directly to the ventral midline (dashed line). Anterior is left; dorsal is up. (C) A *unc-34(lq17); mig-2(mu28)* animal, viewed from a ventral perspective, displayed a PQR neuron that failed to migrate to its final position. Anterior is to the left and the left side of the animal is up. Bars: B, 10 μm; C, 20 μm.

Furthermore, *lq17* animals showed weak defects in PDE axon pathfinding and few AQR/PQR migration defects (Figure 9A). In contrast, other *unc-34* mutants *e951* and *gm104*, both predicted to be null alleles (WITHEE *et al.* 2004), showed stronger defects in PDE axon guidance (9%) and AQR/PQR migration along their normal routes (4–5%) (Figure 9A), but did not affect direction of PQR migration. Thus, *lq17* is likely to be a hypomorphic allele of *unc-34*.

To determine the interactions between *unc-34* and the *rac* genes *ced-10*, *mig-2*, and *rac-2*, we constructed double mutants of *ced-10* and *mig-2* with three *unc-34* alleles, including the hypomorphic *lq17* allele and the null alleles *e951* and *gm104*. Double mutants of *unc-34* and *ced-10* were maintained as double heterozygotes over the balancer *nT1*, which balances both *unc-34* and *ced-10*. Double homozygotes from this balanced strain were viable, but in each case maternal-effect embryonic lethal with the Gex phenotype (data not shown). We scored PDE development and AQR/PQR migration in double mutants with wild-type *unc-34* and *ced-10* maternal contribution. *ced-10(M+); unc-34(e951M+)* and *ced-10(M+); unc-34(gm104M+)* displayed synergistic defects in PDE axon pathfinding and in AQR/PQR migration along their normal routes (Figure 9A). For example, *unc-34(e951)* displayed 9% PDE axon guidance defects whereas *unc-34(e951M+); ced-10(n1993M+)* displayed 40%. *ced-10(n1993M+); unc-34(lq17M+)* displayed a lesser degree of synergy (Figure 9, A–C), supporting the idea that *lq17* is a hypomorphic allele. No defects in the direction of PQR migration were observed.

We analyzed *mig-2(mu28); unc-34* double mutants, which were viable and fertile and did not show strong maternal-effect embryonic lethality. *unc-34; mig-2* animals were severely uncoordinated, and each *mig-2; unc-34* double mutant combination displayed synergistic defects in PDE axon pathfinding and AQR/PQR migration along their normal routes (Figure 9A). Direction of PQR migration was unaffected. These data indicate that while *unc-34* and *mig-2* have overlapping roles in axon pathfinding and neuronal migration, they do not have overlapping roles in embryonic gastrulation.

Finally, to determine if the third *C. elegans rac* gene *rac-2* also acted with *unc-34*, we knocked down *rac-2* function using RNAi in *unc-34(lq17* and *e951)*. We found synergistic defects in PDE axon pathfinding and AQR/PQR

migration in each case (Figure 9A). Direction of PQR migration was not affected in *rac-2(RNAi); unc-34* doubles, and defects with *unc-34(lq17)* were less severe than with *unc-34(e951)*.

These data indicate that mutations in *ced-10*, *mig-2*, and *rac-2(RNAi)* enhance axon pathfinding and AQR/PQR migration defects of null *unc-34* mutants, suggesting that UNC-34 Enabled acts in parallel to *ced-10*, *rac-2*, and *mig-2* in axon pathfinding and neuronal migration. Interestingly, *ced-10(n1993)* and *rac-2(RNAi)* synergized with *unc-34* in gastrulation and embryonic elongation but *mig-2* did not, suggesting that *mig-2* and *unc-34* might act in a common pathway in parallel to *ced-10* and *rac-2* in this event.

MIG-15 NIK and the actin binding protein UNC-115 abLIM act in parallel to UNC-34 Ena in axon pathfinding: The above data are consistent with the idea that three redundant Rac pathways, each using MIG-15 NIK, act in parallel to UNC-34 Ena in axon pathfinding and neuronal migration. If this were the case, we would expect that *unc-34* and *mig-15* mutations would display a synergistic phenotype. In fact, doubles mutants of *unc-34(e951)* with both *mig-15(rh148)* and *mig-15(rh80)* were larval lethal, even with wild-type maternal *mig-15* activity. We were unable to score axon defects in these animals. However, the double hypomorphic mutant *mig-15(rh148); unc-34(lq17)* was viable and severely uncoordinated, and gave rise to some larval lethal animals. The severity of the PDE axon guidance defects in these animals (91%; Figure 5B) was higher than in *mig-15(rh80)* alone and higher than in any *rac; mig-15* double mutant combination. These data indicate that MIG-15 and UNC-34 act in parallel, partially redundant pathways to control axon pathfinding [*i.e.*, *unc-34* enhanced *mig-15* mutations to a level higher than *mig-15(rh80)* alone, whereas *rac* mutations did not]. *unc-34(lq17)* did not enhance defects in the direction of PQR migration or AQR migration of *mig-15(rh148)* (Figure 5C).

The actin-binding protein UNC-115 abLIM (Figure 10A) was previously shown to act downstream of RAC-2 in *C. elegans* axon pathfinding (Struckhoff and Lundquist 2003). If UNC-34 Ena acts in a parallel pathway with Rac signaling, we expect that mutations in *unc-115* and *unc-34* would display synergistic defects in axon pathfinding. We found that double mutants of *unc-115* and *unc-34* were viable and displayed no larval lethality. *unc-115; unc-34* mutants displayed synergistic defects in PDE axon guidance (Figure 10, B and C). For example, *unc-115(ky275)*, a null allele, displayed few PDE axon guidance defects, *unc-34(e951)* displayed 9% defects, and *unc-115(ky275); unc-34(e951)* displayed 33% defects. Double mutants of *unc-115* with *unc-34(lq17)* showed weaker defects, consistent with the idea that *lq17* is a hypomorphic *unc-34* allele.

unc-115; unc-34 double mutants did not display enhanced AQR/PQR migration defects (Figure 10B), nor did they display defects in PQR direction of migration.

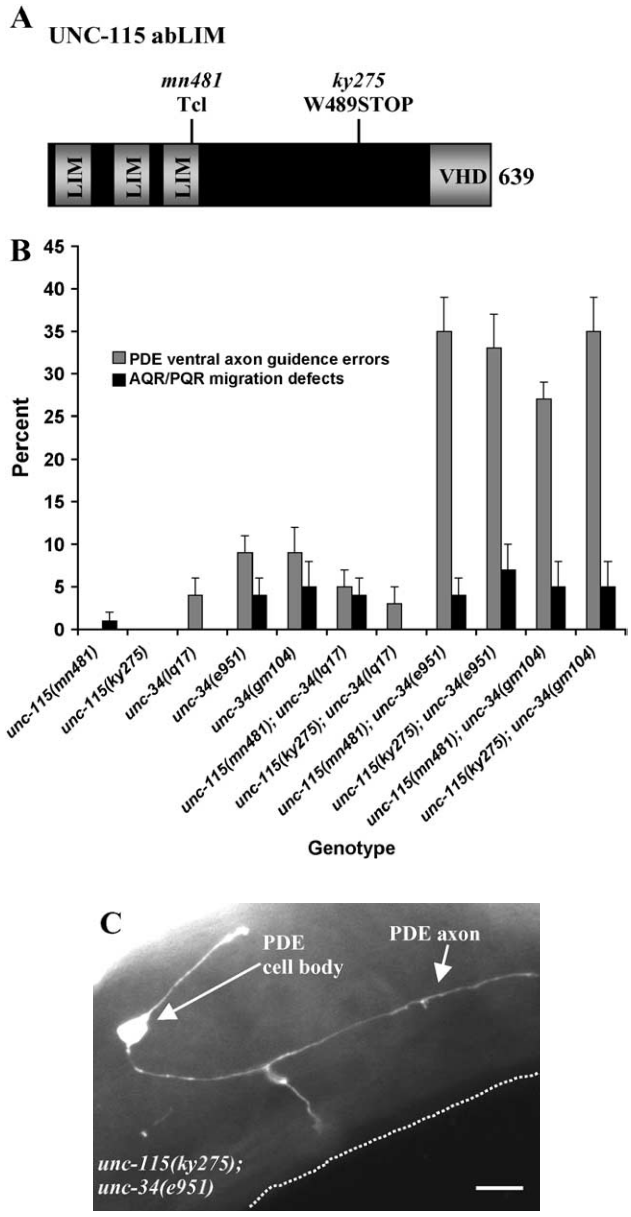

Figure 10.—*unc-115* acts with *unc-34* in PDE axon pathfinding but not AQR/PQR migration. (A) A schematic of the 639-residue UNC-115 polypeptide (GenBank accession no. CAA9005), which contains three N-terminal LIM domains and a C-terminal actin-binding villin headpiece domain (VHD). The locations of the *unc-115* mutations are indicated [*mn481* is a Tc1 transposable element insertion and *ky275* causes a premature stop (Lundquist *et al.* 1998)]. (B) The graph represents percentages of defects (*y*-axis) in various genotypes (*x*-axis). Gray bars represent PDE ventral axon guidance defects and black bars represent AQR/PQR migration defects along their normal routes. Error bars represent the standard error of the proportion. (C) A fluorescent micrograph of an L4 animal with *osm-6::gfp* expression in the PDE neuron. The PDE axon of the *unc-115(ky275); unc-34(e951)* animal failed to extend directly to the ventral midline (dashed line). Bar in C, 10 μm.

This result is consistent with previous studies indicating that *unc-115* does not affect cell migration (*e.g.*, *unc-115* and *rac* mutations showed no enhanced CAN cell migration defects) (Lundquist *et al.* 2001). Thus, UNC-115 might act in parallel to UNC-34 Ena signaling in axon pathfinding but not cell migration.

DISCUSSION

While many signaling molecules that affect axon pathfinding and cell migration have been identified, it is unclear how many of these molecules relate to one another in pathways and networks to control these events. Three Rac GTPases, the MIG-15 NIK kinase, and UNC-34 Enabled have all been shown to affect axon pathfinding and cell migration on their own. Here we present evidence that parallel, partially-redundant pathways control axon pathfinding and neuronal migration in *C. elegans*: three pathways defined by three Rac GTPases and the NIK kinase MIG-15; and another defined by the cytoskeletal signaling molecule UNC-34 Enabled (Figure 11, A and B). The partial redundancy of these pathways in axon navigation indicates that they affect the same cellular process in these events, possibly the organization and dynamics of the actin cytoskeleton of the growth cone that mediates the formation of lamellipodia and filopodia that control growth cone outgrowth and steering. While the three Racs and UNC-34 also redundantly control AQR and PQR migration along their normal routes, MIG-15 was not involved in this event. Rather, MIG-15 acted with MIG-2 to control the direction of PQR migration (Figure 11C).

Three Rac GTPases have overlapping roles in axon pathfinding and neuronal migration: Previous results using a null allele of *mig-2* and a hypomorphic allele of *ced-10* suggested that neither *ced-10* nor *mig-2* had a strong effect on axon pathfinding alone but that the two genes (and *rac-2*) had overlapping roles in axon pathfinding and neuronal migration (Lundquist *et al.* 2001). Here, we analyzed the effects of two deletion alleles of *ced-10* on axon pathfinding, both of which are likely to be null for *ced-10* activity. We found that neither deletion allele resulted in strong defects in axon pathfinding and neuronal migration. While PDE and VD/DD axon outgrowth and AQR/PQR migration occur relatively late in development (in the larva), these events are still subject to maternal contribution [*e.g.*, *mig-15(rh80)* with wild-type maternal *mig-15(+)* activity showed fewer axon and cell migration defects than *mig-15(rh80)* maintained as a homozygous line] (Figure 5B). Therefore, it was possible that *ced-10(+)* maternal activity was masking axon and cell migration defects in *ced-10* null homozygous adults. This is unlikely, as *trans* heterozygotes of *ced-10* deletion alleles and *ced-10(n1993)*, which were viable and fertile and which would have reduced maternal *ced-10* activity, also showed few axon defects (Figure 3A). The *ced-10* deletion alleles strongly synergized with both *mig-2* and

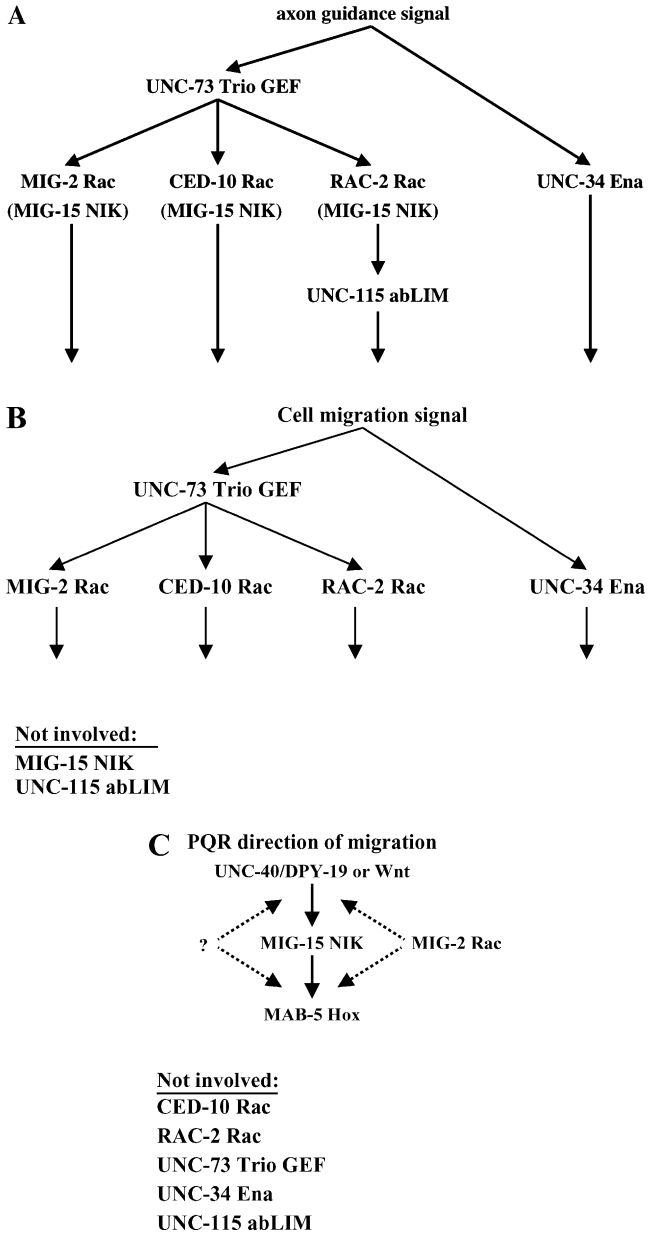

Figure 11.—Models of Rac signaling in axon pathfinding and neuronal migration. (A) PDE ventral axon guidance. Three Rac pathways redundantly control PDE axon guidance. MIG-15 is in parentheses, indicating that MIG-15 might act upstream or downstream of the Racs. UNC-115 acts downstream of RAC-2 Rac. UNC-34 Ena acts in a redundant pathway parallel to the Racs. (B) AQR/PQR migration along their normal routes. The involvement of UNC-34 Ena and the Racs is similar to PDE axon guidance; however, MIG-15 NIK and UNC-115 abLIM are not involved in this process. (C) PQR direction of migration. Initial QL polarity and migration is governed by UNC-40 and DPY-19, and later PQR is polarized by a Wnt signal, which induces MAB-5 expression in PQR and subsequent posterior migration. MIG-15 acts upstream of MAB-5 and might be required for either or both of these polarity events. MIG-2 acts with MIG-15 in controlling PQR direction of migration (upstream or downstream), and another unidentified molecule (?) likely acts in parallel to MIG-2, as *mig-2* mutations alone have no effect on PQR direction of migration. CED-10 Rac, RAC-2 Rac, UNC-73 Trio, UNC-34 Ena, and UNC-115 abLIM are not involved in PQR direction of migration.

rac-2 to cause severe axon defects, indicating that *ced-10*, *mig-2*, and *rac-2* do indeed have overlapping, redundant roles in axon pathfinding and cell migration (Figure 3A).

While the *rac* genes controlled the migration of AQR and PQR along their normal routes, they did not affect the direction of PQR migration. *unc-73* mutations had a similar effect. Thus, our results are consistent with previous results indicating that UNC-73 does not control orientation of Q-cell polarization as do UNC-40 and DPY-19, but rather that UNC-73 is necessary for Q cells to polarize in either orientation (Honigberg and Kenyon 2000). The Racs along with UNC-73 might affect the ability of the Q cells to undergo polarization or the ability of the Q cells or their descendants to migrate along their normal routes.

***mig-2(lq13)*, *ced-10(n1993lq20)*, and *ced-10(n3246)* are gain-of-function *rac* alleles:** We describe the isolation and characterization of gain-of-function alleles of *ced-10* and *mig-2*. Unlike null alleles of each locus, *ced-10(n1993lq20)*, *ced-10(n3246)*, and *mig-2(lq13)* alone affect axon pathfinding and neuronal migration (Figure 7A). Furthermore, transgenic expression of *ced-10* and *mig-2* harboring these mutants led to PDE axon pathfinding defects (Figure 7, B–E). *ced-10(n1993lq20)* was isolated in a hypomorphic *ced-10(n1993)* loss-of-function background. Possibly, the *lq20* mutation could be expressed because of the residual *ced-10* activity in *ced-10(n1993)*, and in a wild-type background the *lq20* mutation might have a much stronger effect. Indeed, transgenic expression of *ced-10(lq20)* without the *n1993* lesion caused strong defects in PDE axon pathfinding. These gain-of-function *rac* mutations also affected AQR and PQR migrations along their normal routes but had no effect on direction of PQR migration.

Constitutive activation of each of the three Racs CED-10, MIG-2, and RAC-2 causes ectopic formation of neurites and ectopic lamellipodia and filopodia formation (Struckhoff and Lundquist 2003), whereas loss of *rac* function (in double mutants) caused axon guidance defects and ectopic neurite formation. The effects of *ced-10(n3246* and *n1993lq20)* and *mig-2(lq13)* mutations in mutants and in transgenic animals resembled *rac* double loss-of-function mutants: axon guidance errors and ectopic neurites with few if any ectopic lamellipodia and filopodia formation (Figure 7). *ced-10(lq20)*, *ced-10(n3246)*, and *mig-2(lq13)* might be dominant-negative rather than a constitutively active alleles, although further experiments will be required to assess the specific effect of each allele. Interestingly, the mutations affect residues in or near the switch regions of the Rac GTPases (Figure 1D). The switch 1 and switch 2 regions mediate interaction of Rac GTPases with their upstream regulators, GTP exchange factors of the DH-GEFs (Erickson and Cerione 2004). In fact, *mig-2(lq13)* affected a residue conserved in human Rac1 that makes a van der Waal's contact with the DH domain of the Rac GEF Tiam1 (Worthylake *et al.* 2000). We have shown previously that the DH-GEF UNC-73 Trio acts in each of the Rac pathways in axon pathfinding and cell migration, and mutations that affect the Rac GEF activity of UNC-73 Trio cause axon and cell migration defects similar to *rac* double mutants. The *n3246*, *lq20*, and *lq13* mutations might cause aberrant interactions of the Rac molecules with UNC-73 Trio that perturb UNC-73 Trio activity in all three Rac pathways. Indeed, dominant-negative T17N Rho GTPase mutants have been shown to interfere with the activity of DH-GEFs, which might be required for multiple Rho GTPase signaling pathways (Debreceni *et al.* 2004).

MIG-15 might act in each of the three Rac pathways in axon pathfinding: *mig-15* encodes a molecule similar to NIK kinase and has previously been shown to affect axon pathfinding (Poinat *et al.* 2002). RNAi of *rac* genes enhanced *mig-15* mutations, suggesting that *mig-15* and the *racs* act together to control axon pathfinding. On the basis of phenotypic and molecular analyses of the *mig-15* mutations presented here, *rh80* and *rh148* likely retain some *mig-15* activity. *rh148* was a missense mutation in the ATP binding pocket of the kinase domain. The residual activity of *mig-15(rh148)* could be due to other domains of the protein (*e.g.*, the CNH domain) or could be due to partial impairment of the kinase domain. *rh80* caused a premature stop in the C-terminal CNH domain. Possibly, the residual activity of *mig-15(rh80)* is due to the activity of the kinase alone (*i.e.*, *rh80* might specifically eliminate the function of the CNH domain but not the kinase domain). *rh326* caused a premature stop in the middle of the reading frame and might be a null *mig-15* allele.

Here we provide genetic evidence that is consistent with the notion that MIG-15 acts in each of the three Rac pathways in axon pathfinding: mutations in *ced-10*, *mig-2*, and *rac-2* enhance a weak *mig-15* allele to resemble the stronger *mig-15(rh80* and *rh326)* alleles; and no *rac; mig-15* double mutant is strikingly more affected than the strong *mig-15(rh326M+)* mutant, although *ced-10(n1993)* might slightly enhance *mig-15(rh326M+)*, raising the possibility that *ced-10* and *mig-15* act in parallel pathways (Figure 5B). MIG-15 physically associates with the INA-1 α-integrin cytoplasmic tail and genetically interacts with INA-1 in axon pathfinding (Poinat *et al.* 2002). Possibly, MIG-15 acts downstream of Racs and affects INA-1 function in response to Rac signaling. Alternatively, INA-1 and MIG-15 might act upstream of Racs and control Rac activity in response to integrin signaling during axon pathfinding.

ced-10 null mutants and *ced-10(n1993); mig-2(mu28)* doubles display synthetic lethality with a Gex phenotype characteristic of defects in cell movements during gastrulation. In contrast, *mig-15* mutants alone and in combination with *mig-2(mu28)* and *ced-10(n1993)* did not display the Gex phenotype, although *ced-10(n1993); mig-15(rh80)* animals were larval lethal. While MIG-15 acts with the Racs in axon pathfinding, it might not act

with the Racs in gastrulation cell movements. However, MIG-15 might have a role in this process that is obscured by redundant gene function.

The Drosophila NIK kinase Misshapen is also involved in cytoskeletal signaling during axon pathfinding (Erickson and Cerione 1993; Ruan *et al.* 1999; Su *et al.* 2000). Furthermore, vertebrate NIK interacts with the SH2-SH3 adapter protein Nck (Su *et al.* 1997), which is a component of a protein complex regulated by Rac activity (Eden *et al.* 2002; Innocenti *et al.* 2004). This complex contains the Arp2/3 activator WAVE/Scar, which induces Arp2/3-dependent actin nucleation in response to Rac signaling (Suetsugu *et al.* 2001). Furthermore, Drosophila Misshapen interacts with the Nck-like molecule Dreadlocks in Drosophila axon pathfinding (Ruan *et al.* 1999). In *C. elegans*, MIG-15 and the Racs might act via a similar signaling mechanism in axon pathfinding.

MIG-15 and MIG-2 control direction of PQR neuronal migration: *mig-15* mutations caused strong anterior misplacement of the QL descendant PQR (Figure 5C), indicating that PQR and/or its precursor QL migrated anteriorly rather than posteriorly. The antennapedia-like homeodomain transcription factor MAB-5 is a key determinant in direction of Q-cell migration: loss of MAB-5 in QL and daughters causes anterior migration rather than the normal posterior; and ectopic expression of MAB-5 in QR and daughters causes posterior migration rather than normal anterior (Salser and Kenyon 1992). At least two events in Q-cell development are required for MAB-5 expression in QL: an initial orientation of QL polarity and migration to the posterior controlled by UNC-40 and DPY-19; and a later posteriorly derived Wnt signal that induces MAB-5 expression in QL and not QR (Honigberg and Kenyon 2000).

Our results suggest that MIG-15 acts upstream of MAB-5 in QL. The gain-of-function *mab-5(e1751)* mutation causes expression of MAB-5 in both QL and QR independent of Wnt signaling, and *mig-15(rh148); mab-5(e1751gf)* double mutants resembled *mab-5(e1751gf)* alone (posterior PQR and posterior AQR). MIG-15 might act in QL downstream of the Wnt signal, or MIG-15 might act in initial Q cell polarity orientation with UNC-40 and DPY-19. Alternatively, MIG-15 might act nonautonomously (*e.g.*, MIG-15 might be required for an inducing cell to secrete a Wnt signal). In Drosophila, the MIG-15-like protein Misshapen acts downstream of the Wnt receptor Frizzled and the Wnt pathway molecule Disheveled in planar cell polarity (Paricio *et al.* 1999).

MIG-15 likely has additional roles in Q-cell development, as both anteriorly directed AQR and PQR often fail to migrate to their normal locations, a defect rarely seen in *mab-5*, *unc-40*, and *dpy-19* mutants. The AQR and PQR migration defects seen in *mig-15* mutants might be due to a defect in cell polarity rather than to a defect in the ability of the cells to migrate. Consistent with this idea, the migration defects of *mig-15* mutants were not enhanced by *ced-10*, *rac-2*, or *unc-34*. Possibly, CED-10, RAC-2, and UNC-34 Ena affect the ability of migrating cells to generate protrusive structures necessary for cell migration (*e.g.*, lamellipodia and filopodia) whereas MIG-15 might be involved in the generation and/or maintenance of cell polarity during migration.

Our data suggest that MIG-2 Rac is involved in both MIG-15–dependent cell polarity and CED-10/RAC-2/UNC-34–dependent cell migration, as *mig-2(mu28)* enhanced the PQR direction of migration defects of *mig-15(rh148)* and synergized with *ced-10(n1993)*, *rac-2(RNAi)*, and *unc-34* for AQR and PQR migration along their normal routes (Figures 3 and 5). MIG-2 has been previously implicated in execution of Q-cell migration and axon pathfinding (Zipkin *et al.* 1997; Lundquist *et al.* 2001) as well as regulating direction of migration of the ray 1 cell in the *C. elegans* male tail in response to semaphorin/plexin signaling (Dalpe *et al.* 2004). Differing levels of Rac activity (including MIG-2) apparently determine whether semaphorin/plexin signaling in ray 1 is attractive (high Rac activity) or repulsive (low Rac activity). Rac activity in ray 1 might involve guided cell and growth cone migration rather than cell polarity *per se* (Dalpe *et al.* 2004). Interestingly, the constitutively-active *mig-2(rh17)* mutation, which presumably causes higher-than-normal levels of MIG-2 activity, affected the ability of Q cells and daughters to execute migrations, similar to *mig-2* loss of function, but did not affect direction of Q-cell migration. Possibly, MIG-2 activity in Q-cell direction of migration is independent of the ability of MIG-2 to cycle between GTP- and GDP-bound forms.

Our data indicate that MIG-15 participates in multiple morphogenetic processes (axon pathfinding and cell polarity), similar to Drosophila Misshapen. In fact, Misshapen acts with distinct signaling networks in the control of axon pathfinding and dorsal closure: axon pathfinding requires Misshapen interaction with the Nck-like protein Dreadlocks, whereas dorsal closure does not (Su *et al.* 2000). Our data suggest that MIG-15 also acts with distinct signaling complexes in different events: MIG-15 acts with the three Rac proteins CED-10, MIG-2, and RAC-2 in axon pathfinding but not in cell migration, and MIG-15 acts with the Rac GTPase MIG-2 in PQR direction of migration, which does not apparently involve CED-10 or RAC-2 (Figure 11).

UNC-34 Ena acts in a parallel, partially overlapping pathway with Rac in axon pathfinding and neuronal migration: In an unbiased screen for new mutations that were synthetic lethal with *ced-10(n1993)*, we identified a new allele of the *unc-34* gene, which encodes the *C. elegans* Enabled molecule (Withee *et al.* 2004). Enabled family members have been broadly implicated in actin organization and cellular morphogenesis, including axon pathfinding (Krause *et al.* 2003). Furthermore,

unc-34 Ena has been previously implicated in axon pathfinding (Gitai *et al.* 2003; Withee *et al.* 2004). We found that null *unc-34* alleles, which were viable and fertile, displayed synthetic lethality with *ced-10(n1993),* and that *unc-34; ced-10* embryos arrested with the Gex phenotype characteristic of defects in cell movements during gastrulation (Soto *et al.* 2002). Thus, UNC-34 and CED-10 might have partially overlapping roles in gastrulation. In contrast, *unc-34; mig-2* doubles were viable and fertile, indicating that UNC-34 and MIG-2 might act in the same pathway in gastrulation or that they both have minor effects on gastrulation compared to CED-10.

We found that *unc-34(lq17)* was a weak hypomorphic allele that had few axon defects on its own but that synergized with *ced-10*, *mig-2*, and *rac-2* for axon pathfinding and AQR/PQR migration along their normal routes (Figure 9A). Previous studies showed that *unc-34* and *ced-10* act redundantly in AVM axon pathfinding (Gitai *et al.* 2003). The *lq17* mutation resulted in the use of a cryptic splice donor site in the last *unc-34* intron (Figure 8, B and C). The polypeptide produced from this transcript is predicted to be missing block C of the EVH2 domain, which is required for Ena tetramerization (Haffner *et al.* 1995; Bachmann *et al.* 1999; Zimmermann *et al.* 2002). Thus, *lq17* might affect the ability of UNC-34 Ena to tetramerize but might leave other functions of the molecule intact. These data suggest that Ena tetramerization is important for the function of the molecule *in vivo*.

unc-34 did not affect direction of PQR migration. Rather, UNC-34 Ena might act in parallel to the Racs and UNC-73 in execution of AQR and PQR migrations along their normal routes. Null alleles of *unc-34*, *e951*, and *gm104* also synergized with *ced-10*, *mig-2*, and *rac-2* for this phenotype. Our data suggest that UNC-34 Ena defines a parallel pathway with partially overlapping function with Rac signaling in axon pathfinding and neuronal migration. In accordance with this model, we found that *unc-34(lq17)* enhanced the axon pathfinding defects of the weak *mig-15(rh148)* allele to a severity higher than the putative null *mig-15(rh326M+)* or any *mig-15; rac* double mutant combination (Figure 5B).

That the Racs and UNC-34 Ena act in a partially overlapping manner in axon pathfinding and neuronal migration suggest that they affect the same process during axon pathfinding. Possibly, both the Racs and UNC-34 Ena drive the formation of protrusive structures (lamellipodia and/or filopodia) in the axonal growth cone and leading edge of a migrating cell in response to guidance and outgrowth signals. Indeed, Enabled controls filopodia formation in neurons in response to axon guidance signals (Lebrand *et al.* 2004), and Rac activity induces both lamellipodia and filopodia in *C. elegans* neurons (Struckhoff and Lundquist 2003). The actin-binding protein UNC-115 abLIM controls lamellipodia and filopodia formation in response to Rac signaling (Struckhoff and Lundquist 2003; Yang and Lundquist 2005), and our results indicate that UNC-34 Ena and UNC-115 act in a partially overlapping manner in axon pathfinding.

The data presented here are consistent with the models presented in Figure 11. In axon pathfinding (Figure 11A), three Rac molecules act redundantly, the NIK kinase MIG-15 might act in each Rac pathway, and the UNC-34 Enabled molecule defines a parallel pathway that acts in a partially overlapping manner with Rac/MIG-15. In AQR/PQR neuronal migration (Figure 11B), the Racs and UNC-34 Ena display similar relationships as in axon pathfinding, although MIG-15 and UNC-115 are not involved in this event. Finally, MIG-2 Rac might act with MIG-15, upstream of MAB-5, in PQR direction of migration in parallel to an unidentified factor. CED-10 Rac, RAC-2 Rac, UNC-73 Trio, UNC-34 Ena, and UNC-115 abLIM are not involved in PQR polarity. In most genotypes described here, many PDE axons are still correctly guided to the VNC, and AQR and PQR are often in their normal locations. In the most severely affected genotype, *mig-15(rh148); unc-34(lq17)*, nearly 10% of PDE axons are still correctly guided to the VNC. These observations suggest that there could be additional parallel pathways that control axon pathfinding and neuronal migration in a partially overlapping manner with Rac/MIG-15 and UNC-34 Enabled.

The authors thank E. Struckhoff and S. Mariano for technical assistance, M. Prochaska for assistance with *mig-15* allele sequencing, M. Herman for critical reading of the manuscript, members of the Lundquist lab for helpful discussions, G. Garriga for *unc-34* strains, S. Mitani and the National Bioresource Project for the Experimental Animal "Nematode *C. elegans*" for *ced-10(tm597),* and the Caenorhabditis Genetics Center, sponsored by the National Center for Research Resources, for *C. elegans* strains. This work was supported by grants from the National Institutes of Health (NIH) (NS40945) and National Science Foundation (IOB93192) to E.A.L., a grant from the National Science Foundation (EPS236913) in support of M.A.S., and NIH grant P30 HD02528.

LITERATURE CITED

Anderson, P., 1995 Mutagenesis. Methods Cell Biol. **48:** 31–58.

Bachmann, C., L. Fischer, U. Walter and M. Reinhard, 1999 The EVH2 domain of the vasodilator-stimulated phosphoprotein mediates tetramerization, F-actin binding, and actin bundle formation. J. Biol. Chem. **274:** 23549–23557.

Brenner, S., 1974 The genetics of Caenorhabditis elegans. Genetics **77:** 71–94.

Collet, J., C. A. Spike, E. A. Lundquist, J. E. Shaw and R. K. Herman, 1998 Analysis of osm-6, a gene that affects sensory cilium structure and sensory neuron function in *Caenorhabditis elegans*. Genetics **148:** 187–200.

Dalpe, G., L. W. Zhang, H. Zheng and J. G. Culotti, 2004 Conversion of cell movement responses to Semaphorin-1 and Plexin-1 from attraction to repulsion by lowered levels of specific RAC GTPases in *C. elegans*. Development **131:** 2073–2088.

Debreceni, B., Y. Gao, F. Guo, K. Zhu, B. Jia *et al.*, 2004 Mechanisms of guanine nucleotide exchange and Rac-mediated signaling revealed by a dominant negative trio mutant. J. Biol. Chem. **279:** 3777–3786.

Dickson, B. J., 2001 Rho GTPases in growth cone guidance. Curr. Opin. Neurobiol. **11:** 103–110.

Dickson, B. J., 2002 Molecular mechanisms of axon guidance. Science **298:** 1959–1964.

Eden, S., R. Rohatgi, A. V. Podtelejnikov, M. Mann and M. W. Kirschner, 2002 Mechanism of regulation of WAVE1-induced actin nucleation by Rac1 and Nck. Nature **418:** 790–793.

Erickson, J. W., and R. A. Cerione, 1993 Regulation of the cGMP phosphodiesterase in bovine rod outer segments. Use of resonance energy transfer to distinguish between associative and dissociative activation mechanisms. J. Biol. Chem. **268:** 3328–3333.

Erickson, J. W., and R. A. Cerione, 2004 Structural elements, mechanism, and evolutionary convergence of Rho protein-guanine nucleotide exchange factor complexes. Biochemistry **43:** 837–842.

Gallo, G., and P. C. Letourneau, 2004 Regulation of growth cone actin filaments by guidance cues. J. Neurobiol. **58:** 92–102.

Gitai, Z., T. W. Yu, E. A. Lundquist, M. Tessier-Lavigne and C. I. Bargmann, 2003 The netrin receptor UNC-40/DCC stimulates axon attraction and outgrowth through Enabled and, in parallel, Rac and UNC-115/AbLIM. Neuron **37:** 53–65.

Haffner, C., T. Jarchau, M. Reinhard, J. Hoppe, S. M. Lohmann *et al.*, 1995 Molecular cloning, structural analysis and functional expression of the proline-rich focal adhesion and microfilament-associated protein VASP. EMBO J. **14:** 19–27.

Hall, A., 1998 Rho GTPases and the actin cytoskeleton. Science **279:** 509–514.

Hatten, M. E., 2002 New directions in neuronal migration. Science **297:** 1660–1663.

Herman, M., 2001 C. elegans POP-1/TCF functions in a canonical Wnt pathway that controls cell migration and in a noncanonical Wnt pathway that controls cell polarity. Development **128:** 581–590.

Honigberg, L., and C. Kenyon, 2000 Establishment of left/right asymmetry in neuroblast migration by UNC-40/DCC, UNC-73/Trio and DPY-19 proteins in *C. elegans*. Development **127:** 4655–4668.

Huber, A. B., A. L. Kolodkin, D. D. Ginty and J. F. Cloutier, 2003 Signaling at the growth cone: ligand-receptor complexes and the control of axon growth and guidance. Annu. Rev. Neurosci. **26:** 509–563.

Innocenti, M., A. Zucconi, A. Disanza, E. Frittoli, L. B. Areces *et al.*, 2004 Abi1 is essential for the formation and activation of a WAVE2 signalling complex. Nat. Cell Biol. **6:** 319–327.

Jin, Y., E. Jorgensen, E. Hartwieg and H. R. Horvitz, 1999 The *Caenorhabditis elegans* gene unc-25 encodes glutamic acid decarboxylase and is required for synaptic transmission but not synaptic development. J. Neurosci. **19:** 539–548.

Kelly, W. G., S. Xu, M. K. Montgomery and A. Fire, 1997 Distinct requirements for somatic and germline expression of a generally expressed *Caenorhabditis elegans* gene. Genetics **146:** 227–238.

Krause, M., 1995 Techniques for analyzing transcription and translation. Methods Cell Biol. **48:** 513–529.

Krause, M., E. W. Dent, J. E. Bear, J. J. Loureiro and F. B. Gertler, 2003 Ena/VASP proteins: regulators of the actin cytoskeleton and cell migration. Annu. Rev. Cell Dev. Biol. **19:** 541–564.

Kriegstein, A. R., and S. C. Noctor, 2004 Patterns of neuronal migration in the embryonic cortex. Trends Neurosci. **27:** 392–399.

Lebrand, C., E. W. Dent, G. A. Strasser, L. M. Lanier, M. Krause *et al.*, 2004 Critical role of Ena/VASP proteins for filopodia formation in neurons and in function downstream of netrin-1. Neuron **42:** 37–49.

Lowe, E. D., M. E. Noble, V. T. Skamnaki, N. G. Oikonomakos, D. J. Owen *et al.*, 1997 The crystal structure of a phosphorylase kinase peptide substrate complex: kinase substrate recognition. EMBO J. **16:** 6646–6658.

Lundquist, E. A., 2003 Rac proteins and the control of axon development. Curr. Opin. Neurobiol. **13:** 384–390.

Lundquist, E. A., R. K. Herman, J. E. Shaw and C. I. Bargmann, 1998 UNC-115, a conserved protein with predicted LIM and actin-binding domains, mediates axon guidance in *C. elegans*. Neuron **21:** 385–392.

Lundquist, E. A., P. W. Reddien, E. Hartwieg, H. R. Horvitz and C. I. Bargmann, 2001 Three *C. elegans* Rac proteins and several alternative Rac regulators control axon guidance, cell migration and apoptotic cell phagocytosis. Development **128:** 4475–4488.

Luo, L., 2000 Rho GTPases in neuronal morphogenesis. Nat. Rev. Neurosci. **1:** 173–180.

Madaule, P., T. Furuyashiki, M. Eda, H. Bito, T. Ishizaki *et al.*, 2000 Citron, a Rho target that affects contractility during cytokinesis. Microsc. Res. Tech. **49:** 123–126.

Madaule, P., T. Furuyashiki, T. Reid, T. Ishizaki, G. Watanabe *et al.*, 1995 A novel partner for the GTP-bound forms of rho and rac. FEBS Lett. **377:** 243–248.

Maloof, J. N., J. Whangbo, J. M. Harris, G. D. Jongeward and C. Kenyon, 1999 A Wnt signaling pathway controls hox gene expression and neuroblast migration in *C. elegans*. Development **126:** 37–49.

Marchler-Bauer, A., J. B. Anderson, P. F. Cherukuri, C. DeWeese-Scott, L. Y. Geer *et al.*, 2005 CDD: a Conserved Domain Database for protein classification. Nucleic Acids Res. **33:** D192–D196.

Mello, C., and A. Fire, 1995 DNA transformation. Methods Cell Biol. **48:** 451–482.

Niefind, K., B. Guerra, L. A. Pinna, O. G. Issinger and D. Schomburg, 1998 Crystal structure of the catalytic subunit of protein kinase CK2 from Zea mays at 2.1 A resolution. EMBO J. **17:** 2451–2462.

Paricio, N., F. Feiguin, M. Boutros, S. Eaton and M. Mlodzik, 1999 The Drosophila STE20-like kinase misshapen is required downstream of the Frizzled receptor in planar polarity signaling. EMBO J. **18:** 4669–4678.

Poinat, P., A. De Arcangelis, S. Sookhareea, X. Zhu, E. M. Hedgecock *et al.*, 2002 A conserved interaction between beta1 integrin/PAT-3 and Nck-interacting kinase/MIG-15 that mediates commissural axon navigation in *C. elegans*. Curr. Biol. **12:** 622–631.

Reddien, P. W., and H. R. Horvitz, 2000 CED-2/CrkII and CED-10/Rac control phagocytosis and cell migration in *Caenorhabditis elegans*. Nat. Cell Biol. **2:** 131–136.

Ruan, W., P. Pang and Y. Rao, 1999 The SH2/SH3 adaptor protein dock interacts with the Ste20-like kinase misshapen in controlling growth cone motility. Neuron **24:** 595–605.

Salser, S. J., and C. Kenyon, 1992 Activation of a *C. elegans* Antennapedia homologue in migrating cells controls their direction of migration. Nature **355:** 255–258.

Sambrook, J., E.F. Fritsch and T. Maniatis, 1989 *Molecular Cloning: A Laboratory Manual*. Cold Spring Harbor Laboratory Press, Cold Spring Harbor, NY.

Soto, M. C., H. Qadota, K. Kasuya, M. Inoue, D. Tsuboi *et al.*, 2002 The GEX-2 and GEX-3 proteins are required for tissue morphogenesis and cell migrations in C.elegans. Genes Dev. **16:** 620–632.

Struckhoff, E. C., and E. A. Lundquist, 2003 The actin-binding protein UNC-115 is an effector of Rac signaling during axon pathfinding in *C. elegans*. Development **130:** 693–704.

Su, Y. C., J. Han, S. Xu, M. Cobb and E. Y. Skolnik, 1997 NIK is a new Ste20-related kinase that binds NCK and MEKK1 and activates the SAPK/JNK cascade via a conserved regulatory domain. EMBO J. **16:** 1279–1290.

Su, Y. C., C. Maurel-Zaffran, J. E. Treisman and E. Y. Skolnik, 2000 The Ste20 kinase misshapen regulates both photoreceptor axon targeting and dorsal closure, acting downstream of distinct signals. Mol. Cell. Biol. **20:** 4736–4744.

Suetsugu, S., H. Miki, H. Yamaguchi, T. Obinata and T. Takenawa, 2001 Enhancement of branching efficiency by the actin filament-binding activity of N-WASP/WAVE2. J. Cell Sci. **114:** 4533–4542.

Sulston, J., and J. Hodgkin, 1988 Methods, pp. 587–606 in *The Nematode Caenorhabditis elegans*, edited by W. B. Wood. Cold Spring Harbor Laboratory Press, Cold Spring Harbor, NY.

Sulston, J. E., and H. R. Horvitz, 1977 Post-embryonic cell lineages of the nematode, *Caenorhabditis elegans*. Dev. Biol. **56:** 110–156.

Tessier-Lavigne, M., and C. S. Goodman, 1996 The molecular biology of axon guidance. Science **274:** 1123–1133.

Treisman, J. E., N. Ito and G. M. Rubin, 1997 Misshapen encodes a protein kinase involved in cell shape control in Drosophila. Gene **186:** 119–125.

Whangbo, J., and C. Kenyon, 1999 A Wnt signaling system that specifies two patterns of cell migration in *C. elegans*. Mol. Cell **4:** 851–858.

White, J. G., E. Southgate, J. N. Thomson and S. Brenner, 1986 The structure of the nervous system of the nematode *Caenorhabditis elegans*. Philos. Trans. R. Soc. Lond. **314:** 1–340.

Withee, J., B. Galligan, N. Hawkins and G. Garriga, 2004 *Caenorhabditis elegans* WASP and Ena/VASP proteins play compensatory roles in morphogenesis and neuronal cell migration. Genetics **167:** 1165–1176.

Worthylake, D. K., K. L. Rossman and J. Sondek, 2000 Crystal structure of Rac1 in complex with the guanine nucleotide exchange region of Tiam1. Nature **408:** 682–688.

Wu, Y. C., T. W. Cheng, M. C. Lee and N. Y. Weng, 2002 Distinct rac activation pathways control *Caenorhabditis elegans* cell migration and axon outgrowth. Dev. Biol. **250:** 145–155.

Yang, Y., and E. A. Lundquist, 2005 The actin-binding protein UNC-115/abLIM controls formation of lamellipodia and filopodia and neuronal morphogenesis in *Caenorhabditis elegans*. Mol. Cell. Biol. **25:** 5158–5170.

Zimmermann, J., D. Labudde, T. Jarchau, U. Walter, H. Oschkinat *et al.*, 2002 Relaxation, equilibrium oligomerization, and molecular symmetry of the VASP (336–380) EVH2 tetramer. Biochemistry **41:** 11143–11151.

Zipkin, I. D., R. M. Kindt and C. J. Kenyon, 1997 Role of a new Rho family member in cell migration and axon guidance in *C. elegans*. Cell **90:** 883–894.

Communicating editor: K. Kemphues